CORRELATION OF MICROSTRUCTURE WITH TENSILE DEFORMATION BEHAVIOUR IN DISPERSION STRENGTHENED ALUMINUM

BY

NARENDRA SINGH SURANA
B. Sc. (Met-Engg.), Banaras, H. University, 1965

A THESIS SUBMITTED IN PARTIAL FULFILMENT OF
THE REQUIREMENTS FOR THE DEGREE OF
MASTER OF APPLIED SCIENCE

in the Department
of
METALLURGY

We accept this thesis as conforming to the
standard required from candidates for the
degree of MASTER OF APPLIED SCIENCE.

THE UNIVERSITY OF BRITISH COLUMBIA

May, 1967

In presenting this thesis in partial fulfilment of the requirements for an advanced degree at the University of British Columbia, I agree that the Library shall make it freely available for reference and study. I further agree that permission for extensive copying of this thesis for scholarly purposes may be granted by the Head of my Department or by his representatives. It is understood that copying or publication of this thesis for financial gain shall not be allowed without my written permission.

Department of Metallurgy

The University of British Columbia
Vancouver 8, Canada

Date May 5, 1967

ABSTRACT

The tensile behaviour of an Al-10Sb alloy, containing a dispersion of the intermetallic compound AlSb, has been compared with that of an overaged Al-4Cu alloy in the temperature range of -100 to 200°C. As an aid to the interpretation of the alloy results, pure aluminum has also been examined, over the range of grain size represented by the two alloys.

A coarse dispersion of AlSb was not found to increase the yield strength of aluminum for a given initial grain (or subgrain) size. However, the dispersion markedly increased the resistance of aluminum to recovery and recrystallisation, at the same time increasing the true ultimate strength and the uniform elongation. The observed tensile properties of pure aluminum have been explained by a cell formation and migration argument. The tensile deformation behaviour of Al-10Sb and Al-4Cu has been explained in the light of current theories and as an extension of the interpretation of the behaviour of pure aluminum.

ACKNOWLEDGEMENTS

The author wishes to express his sincere gratitude, to Dr. J. A. Lund, for his advice and assistance, through the preparation of this thesis. He also wishes to express his thanks to Dr. R. Warda for his helpful suggestions during this work.

The author wishes to thank the members of the faculty and fellow graduate students of the Department of Metallurgy for many helpful discussions.

Special thanks are extended to Messers. A. Lacis and P. Musil for their assistance in metallography, and to the technical staff of the department for their valuable assistance.

Financial assistance provided by the Defence Research Board and National Research Council is gratefully acknowledged.

TABLE OF CONTENTS

Table of Contents (Cont.)

LIST OF FIGURES

List of Figures (Con't)

List of Figures (Cont.)

LIST OF TABLES

I INTRODUCTION

Dispersion Strengthening Approaches

Precipitation hardened alloys owe much of their strength to a fine dispersion of a sub-precipitate, or "zones". Many of these alloys continue to exhibit relatively high strength even after coherency strains have been eliminated by overaging. Dispersion strengthened alloys of this group are "solution-treatable", i.e., the dispersed second phase must be soluble in the solid matrix at some elevated temperature. Even at temperatures below that at which they dissolve completely, the second phase particles will have a tendency to reduce their surface area by coarsening, or coalescence. Since the strengthening effect of a dispersion is strongly dependent upon the particle spacing, such coarsening invariably causes a decrease in alloy strength. Therefore, the structure and mechanical properties of dispersion strengthened alloys produced by solute rejection from solid solution are inherently unstable at elevated temperatures.

Various methods for the production of dispersion strengthened alloys containing a more stable second phase have been discussed by Grant[1]. Of these, two methods have received considerable attention:

(i) Incorporating an oxide in a metal matrix by powder metallurgical techniques or internal oxidation of a suitable alloy. Since the discovery of "Sintered Aluminum Powder" (SAP) by Irmann[2], there has been considerable activity in this field.[3-8]

(ii) Incorporating (in a metal matrix) a dispersion of an "insoluble" intermetallic compound formed during the solidification of a suitable alloy. High rates of solidification are desirable to obtain a fine dispersion. Thus, powders obtained by a melt fragmentation technique, e.g., atomising, are a

suitable starting material.

Towner[9] undertook a general comparative study of the two methods, applied to aluminum. He reported that alloys having a dispersion of an intermetallic compound during rapid solidification of the alloy have somewhat lower strength properties but significantly higher ductility (especially at elevated temperatures) as compared to alloys containing a dispersion of oxide.

Alloys containing fine dispersions of "insoluble" intermetallic compounds offer the promise of higher strength levels at elevated temperatures than age-hardening alloys by virtue of their greater structural stability.

Probably the most effective way to ensure that a uniform, fine intermetallic compound dispersion is provided by solidification is to employ an alloy of eutectic or near eutectic composition. It is a basic requirement that the eutectic be formed between an intermetallic compound of unique composition and a pure metal. Solubility of the two eutectic phases in each other should be negligibly low, if possible, at all temperatures below the eutectic isotherm. This is essential to structural stability. Moreover, the volume fraction of the intermetallic dispersion in the alloy should not be more than about 15%, or the ductility of the alloy is unlikely to be satisfactory. Among the other requirements of a suitable alloy system are the following:

(1) The melting point of the intermetallic should be high so that it does not lose strength appreciably at elevated temperatures.

(2) The melting point of the eutectic should not be much lower than that of the pure metal on which the alloy is based; otherwise the working temperature range of the alloy would be reduced substantially relative to

the pure solvent.

(3) The morphology of the eutectic should be of the divorced type[10], with essentially equiaxed or spheroidal particles of the intermetallic phase, uniformly dispersed in the metal matrix.

Spengler[11] has proposed that divorced eutectics are formed when two parameters θ and ϕ are both less than 0.1 where

$$\theta = \frac{T_1 - T_E}{T_2 - T_E}$$

T_1 = Melting temperature of the lower melting phase

T_2 = Melting temperature of the higher melting phase

T_E = Eutectic temperature

and $$\phi = \frac{\phi_2}{\phi_1}$$

ϕ_2 = Volume fraction of the higher melting phase

ϕ_1 = Volume fraction of the lower melting phase

Although the reliability of these empirical criteria is open to question[12-13], they can be employed as rough guides to the selection of suitable alloy systems. In fact the tendency to the formation of a divorced type of eutectic is increased at the rapid rates of solidification which are of interest in the present work.

Many systems (e.g. Aluminum-Nickel, Aluminum-Antimony, Aluminum-Iron, Aluminum-Cobalt, Magnesium-Silicon) satisfy most of the aforementioned requirements.

Of these systems, the Al-Sb system has been chosen for inclusion in the present study. Part of the Al-Sb phase diagram is reproduced in Figure 1 from Hansen[14], incorporating a correction given by Elliott[15]. The solid solubility of antimony in aluminum in the range 200 - 645°C is less than 0.10% antimony. The compound AlSb is reported[16] to have a cubic structure of the ZnS type with a lattice parameter of 6.1355 ± 0.0001 A°.

Scope of the Present Investigation

Powder metallurgical procedures were involved in fabricating an alloy containing a fine dispersion of an intermetallic compound. It was found that the matrix grain size was invariably very fine in such material, particularly when compared to the matrix grain size in a solution-treated and overaged alloy. As a result, it was necessary to try to isolate the effect of grain boundaries on tensile behaviour in the temperature range of interest. This was done by studying the behaviour of pure aluminum in a fairly wide range of grain size.

The scope of the present work thus embodied the following:

(1) Effect of matrix grain size on the tensile properties and work-hardening behaviour in the temperature range 0.2 to 0.5 Tm (Tm, the melting point of matrix metal in degrees Kelvin) for a dispersion strengthened material involving a dispersion of an intermetallic compound formed during rapid solidification.

(2) Variation of the tensile properties and work-hardening behaviour of pure polycrystalline aluminum with grain size in the temperature range of 0.2 to 0.5 Tm.

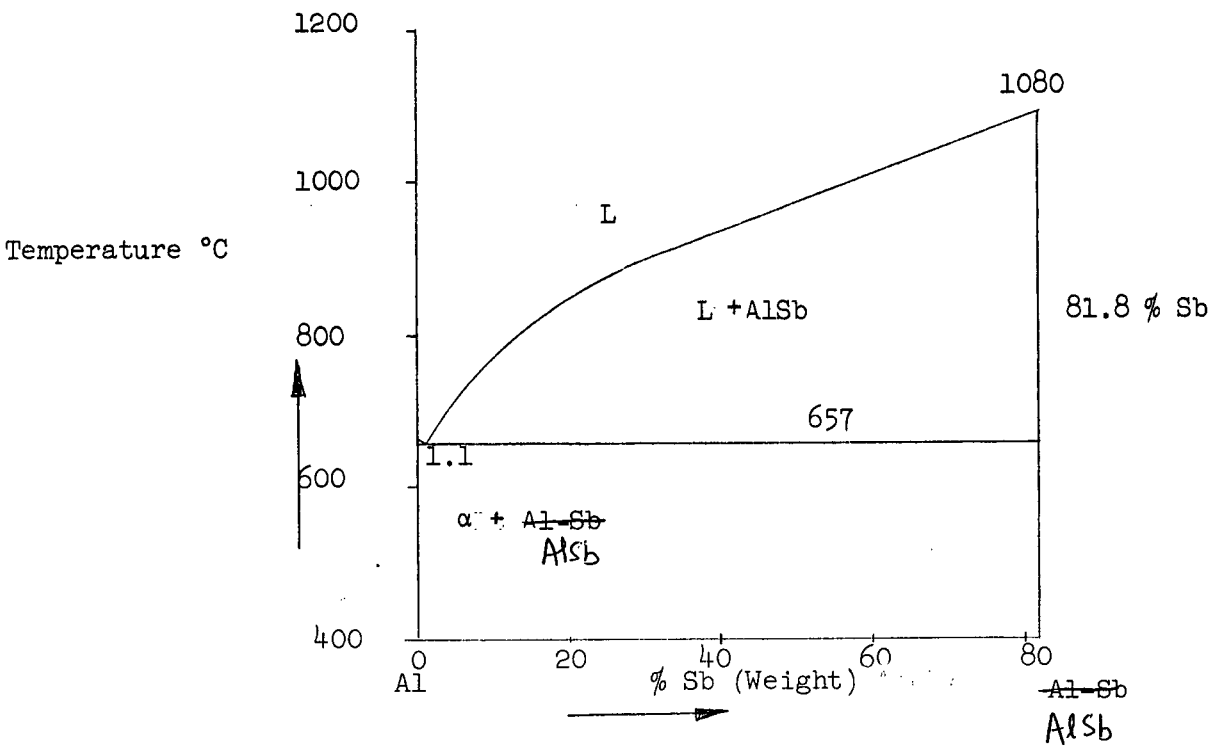

Figure 1. Al-Sb Phase Diagram

(3) Comparison of a fine grained alloy containing a coarse dispersion of a thermally stable intermetallic compound with a coarse grained alloy containing a fine dispersion of a thermally unstable compound with regard to their tensile properties and work-hardening behaviour in the temperature range of -100°C to +200°C.

II EXPERIMENTAL

Materials

Superpurity aluminum was supplied by the Aluminum Company of Canada in the form of 25 lb ingots, the analysis of which is shown in Table 1.

Antimony was supplied by J.T. Baker Chemical Co., Phillipsburg, N.J., in the form of lumps, the analysis of which is shown in Table 2.

Reagent grade copper shot from Fisher Scientific (meeting A.C.S. specifications) containing Cu_{min} 99.99% was used for alloying with superpurity aluminum.

Melting and Solidification

Aluminum and alloys were melted in silicon carbide crucibles. In preparing an alloy, pure aluminum was melted first, the alloying element was added, and the melt was stirred. The temperature of the melt was maintained at 50 to 70°C above the liquidus temperature of the alloy. The melt was given occasional stirring to enhance dissolution. In the case of pure aluminum, the temperature of the furnace was maintained at 710 to 730°C following a gradual heating of the charge.

Rapid solidification was brought about by two different methods:

Table I

Analysis of Aluminum Used

Cu	Fe	Si	Mg	Al (by difference)
.001	.002	.001	.004	99.992

Table 2

Analysis of Antimony Used

Fe	As	Pb	Cu	Sb (by difference)
.002	.004	.004	.002	99.988

(1) Chill Casting:

In a 1" diameter by 3" long split copper mould.

(2) Shotting:

To get solidification rates higher than those possible in chill casting, a shotting technique was employed. Melts of the desired composition were made to pass through a fine orifice under pressure and the issuing stream was quenched in water. The equipment used for this purpose is sketched in Figure 2.

Graphite was used for the container mainly because of its good machinability. A replaceable graphite bottom was machined to screw-fit into the crucible, and had a 0.020" diameter hole drilled in it.

The melting furnace was set close to the shotting equipment. As soon as the melt was ready, the lid of the container was lifted and the melt poured into it. Argon gas pressure on the melt was gradually increased to a level where good spherical shot was found to be obtained by experience. This occured at a gauge pressure of about 25 pounds per square inch.

Shot was recovered from the water, washed repeatedly in alcohol, and stored in an evacuated dessicator to minimise surface oxidation prior to use.

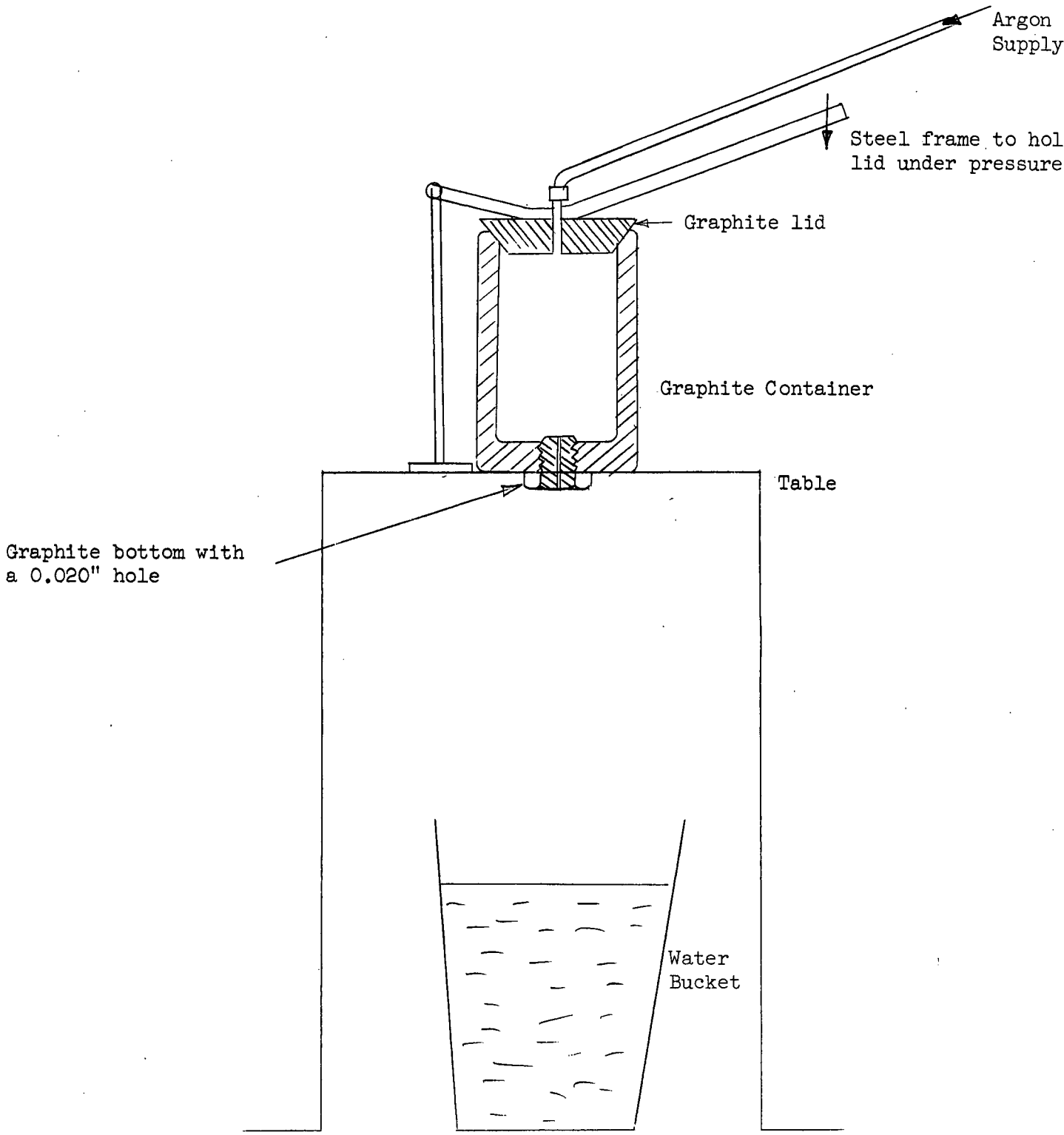

Figure 2. Shotting Equipment

Fabrication

Shot was converted to wrought material in two stages, compacting and extruding, whereas cast materials were extruded directly.

Compacting:

The shot was statically cold compacted to obtain billets of 3/4" diameter. Pressures of about 100,000 p.s.i. were employed. A thin layer of lubricant (containing Molybdenum disulphide) was applied to components of the compacting dies, but due care was taken to minimise entrapment of lubricant in the compacts. Compacts were degreased and throughly cleaned in chlorothene (tri-chloro-ethylene) using a supersonic vibratory cleaner.

Extrusion:

Cast or compacted billets of 3/4 inch diameter were hot extruded to wires of 0.15 inch diameter. The extrusion ratio was 25 to 1. The container, together with die, plugs and ram was preheated "in situ" by an electric resistance-heated sleeve. To minimise the oxidation of aluminum billets, particularly the internal oxidation of shot compacts, billets were put in the container only when the whole assembly had reached the desired extrusion temperature. The first few inches of each extrusion was discarded and the last 1/2 to 3/4 inches of each billet was not extruded.

Tensile Specimens

A small precision lathe was used for machining tensile specimens from extruded wire. The specimens were machined to a

reduced diameter of 0.100" in a gauge length of 1 inch.

Next the specimens were placed in ~~a groove~~ grooves on the top surface of a firebrick, and annealed in a muffle furnace. The specimen-brick assembly was allowed to cool in air after removal from the furnace.

In the case of aluminum - 4% copper, solution treatment was done in a tube furnace at 535 $\pm$ 5° C. Aging was then carried out at 300 $\pm$ 5°C for 60 minutes in a tube furnace.

Tensile Tests

All tensile tests were performed on a Instron tensile testing machine. Threaded "tap wrench" grips were used in most cases. In the case of the coarsest-grained aluminum, where slippage in the mechanical grips was observed, specimens were cemented into hollow-ended grips using an epoxy resin.

Four test temperatures were used: -100°C, Room Temperature, 100°C and 200°C, covering the range of 0.19 to 0.51 Tm. (of aluminum). Petroleum ether, cooled with liquid nitrogen was used for the lower temperature. For higher temperature tests specimens and grips were immersed in a heated silicon oil bath. A controller incorporated in the heating circuit maintained temperatures of 100 $\pm$ 1°C and 200 $\pm$ 2°C.

Tension tests at all temperatures were performed at a strain rate of 0.33×10^{-3} sec.$^{-1}$. In addition some room temperature tests were performed at strain rates of 0.33×10^{-4} sec.$^{-1}$ and 0.33×10^{-2} sec^{-1}.

Metallography

Optical Microscopy:

Specimens to be examined were mounted in "Koldmount" self-curing resin and polished on a series of emery papers. The specimens were then electropolished in a solution of composition - Nitric acid - 1 part, Methyl alcohol - 1 part, Hydrochloric acid - 1 ml per 50 ml of the mixture. The electropolishing solution was prevented from heating by means of water-cooling coils around the beaker, and was stirred by a magnetic stirrer. A stainless steel beaker served as the cathode. A good polish was obtained at 3 volts.

Different etchants were necessary to reveal the microstructure of different materials. Coarse grained aluminum was effectively etched by immersing the specimen for 15-20 seconds in a 10% sodium hydroxide solution heated to 70° C. Aluminum - 4% copper (Overaged, as well as solution treated) was etched electrolytically in the polishing solution simply by turning down the voltage to 1.5 V. The structure of medium grain sized aluminum was best revealed by anodising the electropolished surface in a 1.8% solution of fluoboric acid (HBF_4) at 50 V and using an aluminum cathode. The anisotropic but epitaxial oxide layer was then examined under polarised light. The details of this technique are discussed by Barker.[17]

Electron Microscopy:

Electron miscroscopy was used to study the microstructures of very fine grained aluminum and the aluminum - 10% antimony alloy.

Strips of about 0.007" to 0.010" thickness were spark machined from extruded wires parallel to the extrusion direction. Strips were electro-polished and thinned using the same polishing solution as described above. Thin films were examined using an Hitachi HU-11A Electron Microscope.

A replica technique was used with some specimens. A negative cellulose acetate replica was dry-stripped from a polished and etched specimen surface. Chromium was then deposited at an angle of 45 degrees to the surface of the cellulose acetate, followed by the deposition of a thin film of carbon normal to the surface. The cellulose acetate was then dissolved away using acetone, leaving the carbon replica with the chromium shadowing intact.

Measurement of Grain-Size

Fullman[18] has shown that the diameter d of spherical grains is related to the mean lineal traverse length $\bar{l}$ at any section as follows:

$$d = 1.5\ \bar{l}$$

For the purpose of determining the size of equiaxed grains the above relationship should be applicable reasonably well and was the one used generally in the present work.

Some of the "grains" were found to be elongated in low-temperature extrusions. The essential arguements of Fullman[18] can be used to develop the following relations for this case:

In three dimensions the "grains" can be approximated to rods. The longer dimension is in the extrusion direction as well as the tensile direction, and is perpendicular to the direction of examination.

Figure 3 is a sketch of a rod-shaped grain. PQRS and ABCD are sections parallel to the longer dimension of the grain. If the electron miscroscope foils are prepared parallel to the longer dimension of the rods then sections visible in the microstructure would be those parallel to PQRS and ABCD.

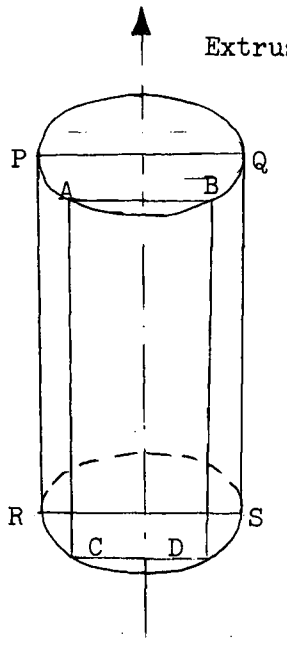

Figure 3. Sketch of a rod shaped grain

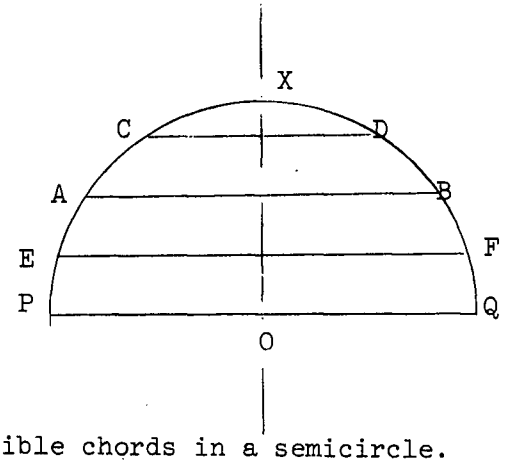

Figure 4. Width of possible chords in a semicircle.

In Figure 4 the average width of all the possible chords e.g. AB, CD, EF, PQ, etc. in a semicircle can be shown mathematically to be:

$$\text{Average width} = \frac{\pi d}{4}$$

where d is the rod diameter.

Since the probability of seeing any particular chord as the shorter dimension of a rectangular section in the microstructure is the same as that of any other chord, by averaging the shorter dimensions of the "grains" from the microstructure the actual diameter of the "grains" is three dimensions could be estimated reasonably well.

The direction along which slip occurs within any grain is assumed to be at an angle of 45° to the load axis. Thus the average width $\bar{l}$ of the elongated grains is related to the effective diameter of the grains as:

$$d_{\text{effective}} = \frac{\sqrt{2}}{(\pi/4)} \bar{l}$$

$$= 1.8\, \bar{l}$$

III OBSERVATIONS AND RESULTS

Metallographic Observations:

Results of the measurement of "grain" size on different materials are collected in Table 3. Some features of the microstructure are dealt with in the following sections, whereas more detailed interpretations follow in the Discussion Section.

(1) 2.7 μm Pure Aluminum (extruded from shot)

Typical transmission electron micrographs of the 2.7 μm pure aluminum are shown as Figures 5 through 8. In these micrographs only a few "grains" exhibit any significant difference in their transparency to electrons compared to other "grains" in the area represented. This indicates that most of the "grains" in each area were misoriented at relatively small angles to one another. This observation was confirmed by a limited number of selected area diffraction patterns on adjacent "grains". The misorientation was less than 5° in each case.

The term "grains" will be used henceforth for any regions in the microstructure that are separated by distinguishable boundaries, regardless of the magnitude of the misorientation across the boundaries.

Grains in Figure 5 have relatively sharp boundaries and few cells of dense dislocations, whereas the boundaries in Figures 6, 7 and 8 are less distinct and there are more dislocations evident, mainly near the boundaries.

Table 3

Grain Size of Materials Investigated

Material	Solidification, Working and Thermal History	Grain Size in μm
Pure Al	Shot, Cold Compacted, Extruded at 200 °C Annealed at 200 °C For 1 hr.	2.7
Pure Al	Chill Cast, Extruded at 200 °C and annealed at 200 °C for 1 hr.	3.5
Pure Al	Chill Cast, Extruded at 300 °C and annealed at 300 °C for 1/2 hr.	10
Pure Al	Chill Cast, Extruded at 400 °C and annealed at 400 °C for 1/2 hr.	98
Al-10Sb	Shot, Cold Compacted, Extruded at 300 °C and annealed at 300 °C for 1/2 hr.	2.9
Al-4Cu	Chill Cast, Extruded at 300 °C, Sol^{n} treated at 535 °C for 4 hr. and overaged at 300 °C for 1 hr.	220
Al-4Cu	Chill Cast, Extruded at 300 °C and solution treated at 535 °C X 4hrs. 25 mts.	270

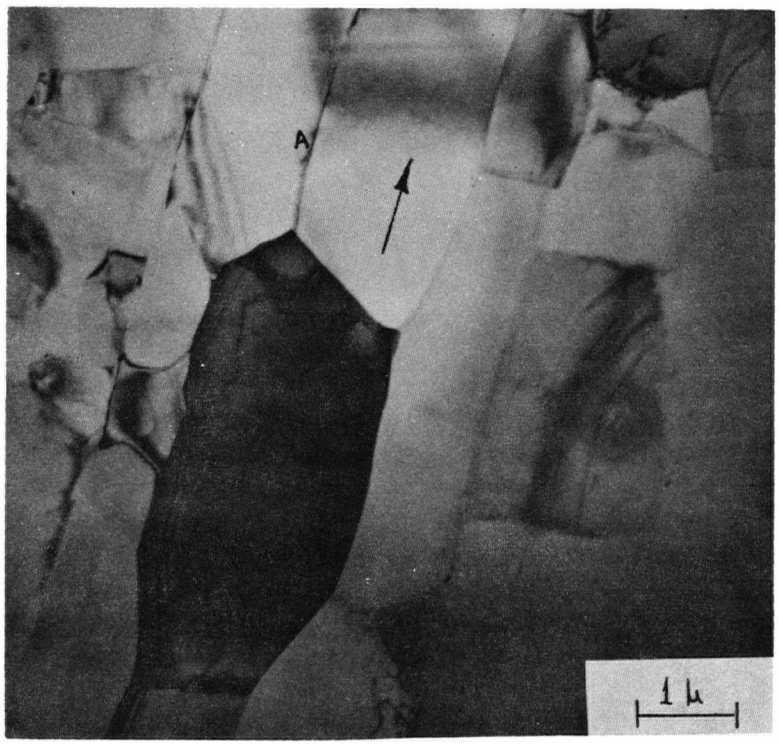

Figure 5. Transmission electron micrograph of 200°C extruded and annealed aluminum from shot.

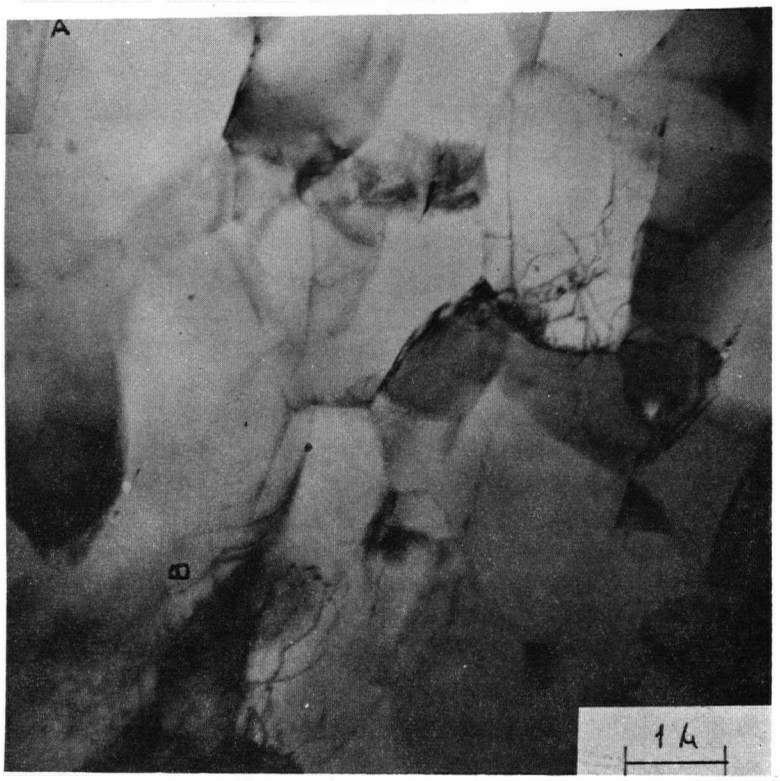

Figure 6. Transmission electron micrograph of 200°C extruded and annealed aluminum from shot.

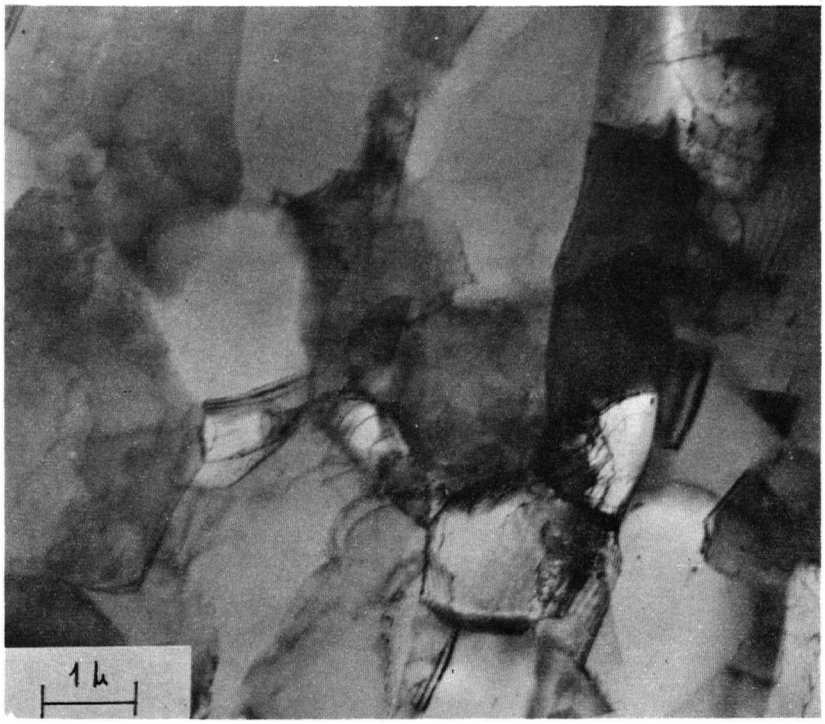

Figure 7. Transmission electron micrograph of 200°C extruded and annealed aluminum from shot.

Figure 8. Transmission electron micrograph of 200°C extruded and annealed aluminum from shot.

Some of the grains appear to be elongated in Figure 5, (direction marked with the arrow) whereas they appear to be comparatively equiaxed in Figures 6 through 8. This has placed a limitation of the accuracy with which grain diameter could be estimated.

Any entrapped aluminum oxide (originating on the surface of shot) was apparently dispersed sufficiently coarsely in the microstructure that it could not be detected as such by transmission microscopy. It is therefore unlikely that oxide in this material contributed significantly to deformation behaviour.

(2) 3.5 μm Pure Aluminum (extruded from billet)

Typical thin film electron micrographs of the 3.5 μm pure aluminum are shown in Figures 9 through 12. Contrast differences between adjacent grains were not distinct in all areas but on the average were greater than those observed in the 2.7 μm aluminum. Similarly the grain boundaries were sharper, and fewer dislocation aggregates were seen in the microstructure. In the areas examined, the grains were found to be relatively equiaxed.

(3) 10 μm Pure Aluminum

Typical optical micrographs of the 10 micron aluminum (after anodising and using polarised light) are shown as Figures 13 and 14).

The grains were all equiaxed. The contrast between adjacent grains was sharp. This suggests that recrystallised grains had formed which is expected as a result of a 300°C anneal[19].

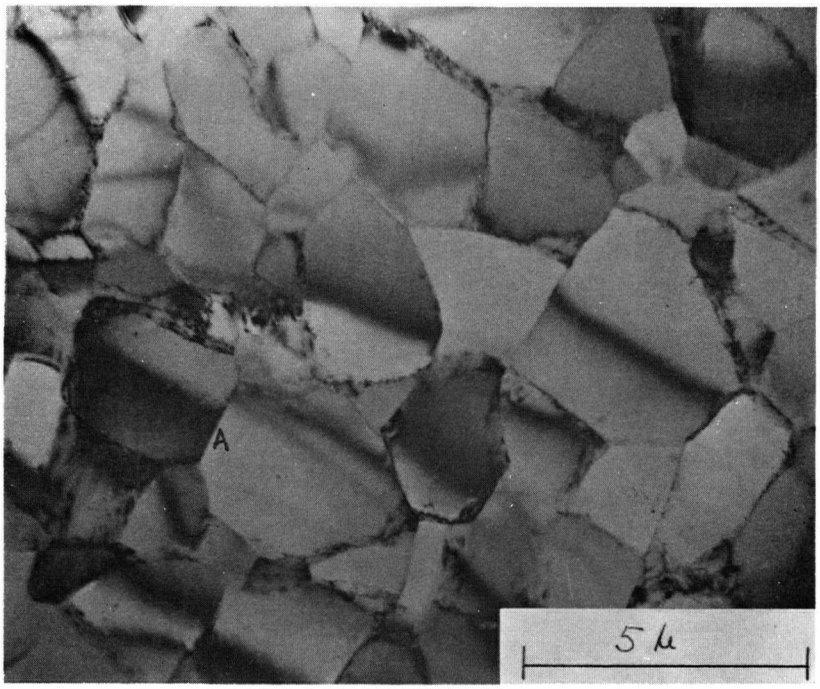

Figure 9. Transmission electron micrograph of 200°C extruded and annealed aluminum from cast billet.

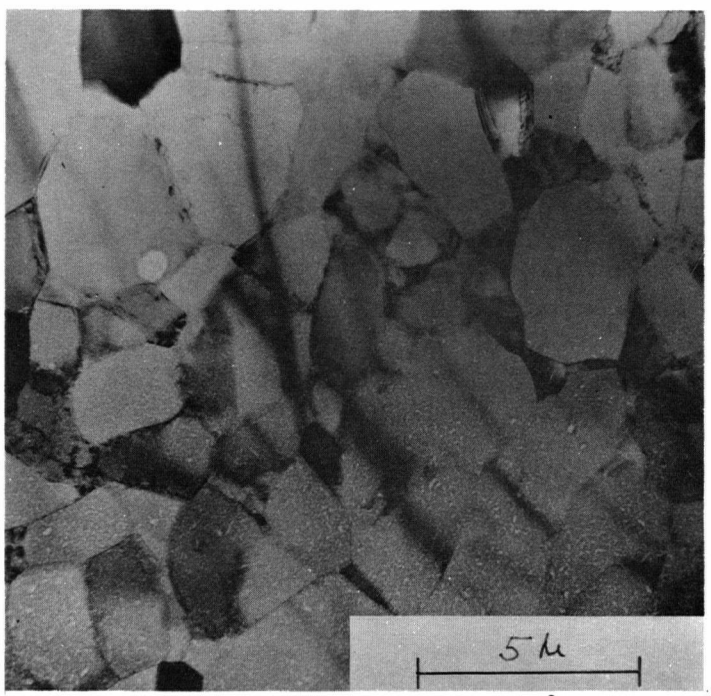

Figure 10. Transmission electron micrograph of 200°C extruded and annealed aluminum from cast billet.

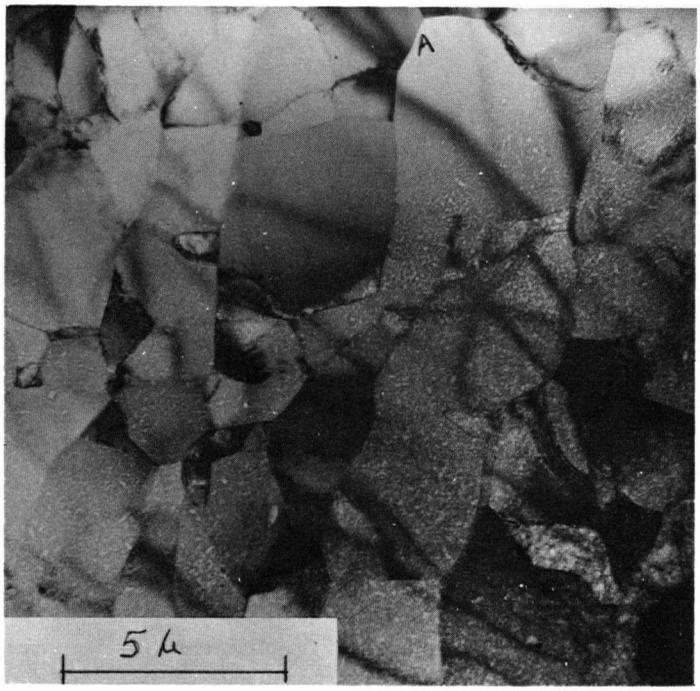

Figure 11. Transmission electron micrograph of 200°C extruded and annealed aluminum from cast billet.

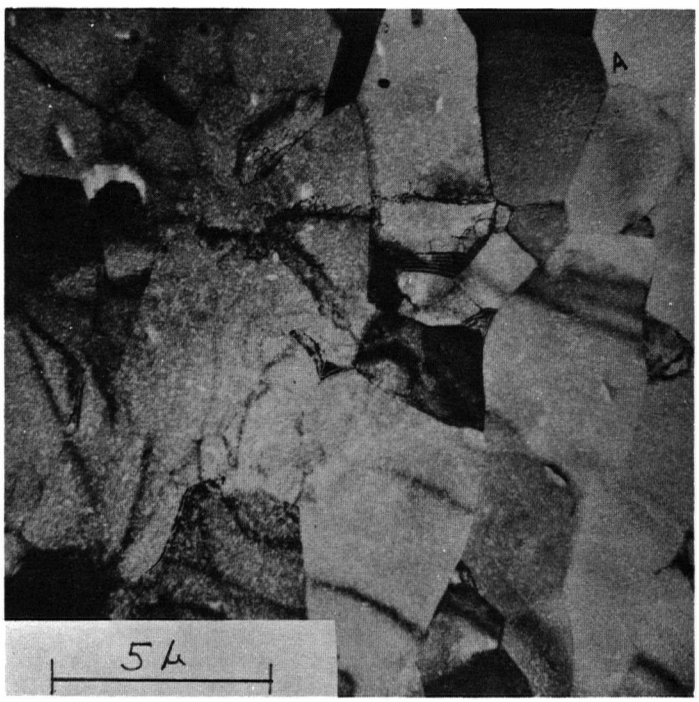

Figure 12. Transmission electron micrograph of 200°C extruded and annealed aluminum from cast billet.

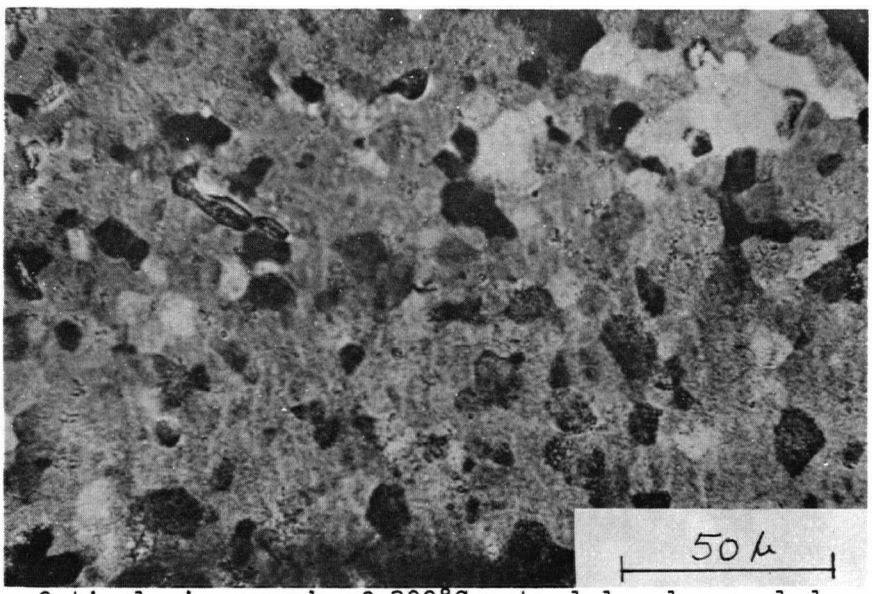

Figure 13. Optical micrograph of 300°C extruded and annealed aluminum using polarised light on anodised surface.

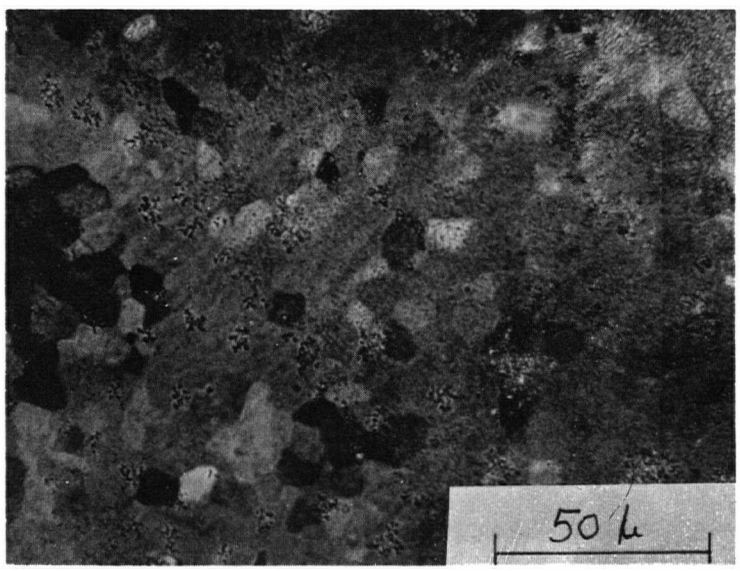

Figure 14. Optical micrograph of 300°C extruded and annealed aluminum using polarised light on anodised surface.

(4) 98 μm Pure Aluminum

Typical optical micrographs of 98 μm pure aluminum are shown in Figures 15 through 17. Most of the grains are equiaxed, although some exceptions are apparent. The grain boundaries were generally sharply revealed.

(5) Aluminum - 10% Antimony

Figures 18 through 21 are transmission electron micrographs of areas which reveal the matrix grain boundaries in the Al-10% Sb. The lack of contrast between adjacent grains suggest that many of the boundaries are probably of low angle. The boundaries are not sharp, and some grains contain dislocation sub-structures.

The particles of AlSb appear black where they were retained in the foil at the time of examination. White areas are believed to correspond to where AlSb particles at the surface have been extracted in the electropolishing operation. All the AlSb particles were found to lie either on, or very close to the matrix grain boundaries.

Figures 22 and 23 are from areas in which the intermetallic particles of AlSb were more clearly detectable. Most of the particles did not have any one dimension particularly larger than any other dimension. The particles tended to be angular in shape, although the corners of some were rounded, possibly during electropolishing.

Figures 24 and 25 are micrographs of replicas taken from different areas to emphasise the observation that the AlSb dispersion was not very uniform - particularly with respect to the size of the AlSb particles.

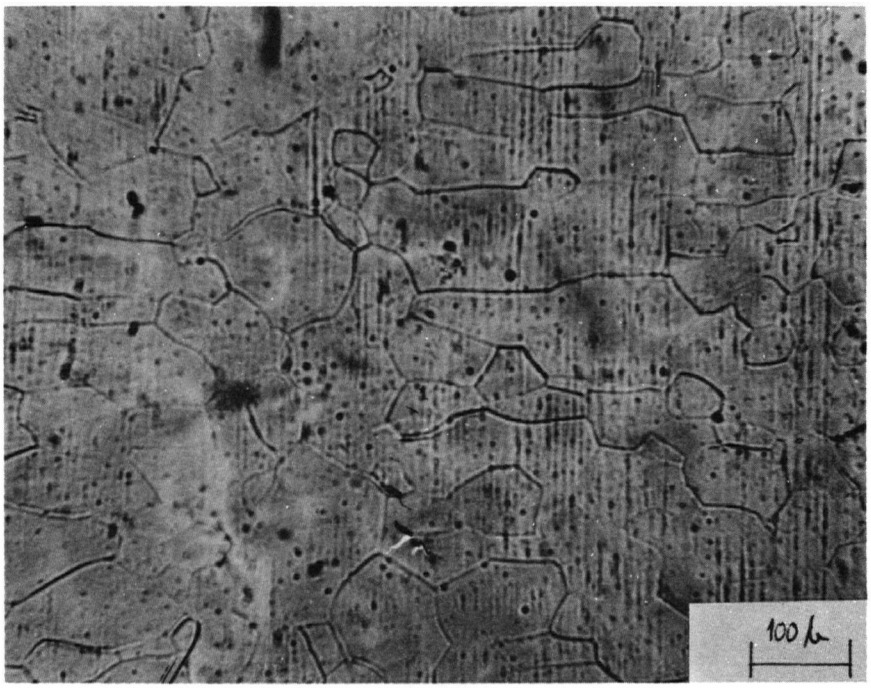

Figure 15. Optical micrograph of 400°C extruded and annealed aluminum.

Figure 16. Optical micrograph of 400°C extruded and annealed aluminum.

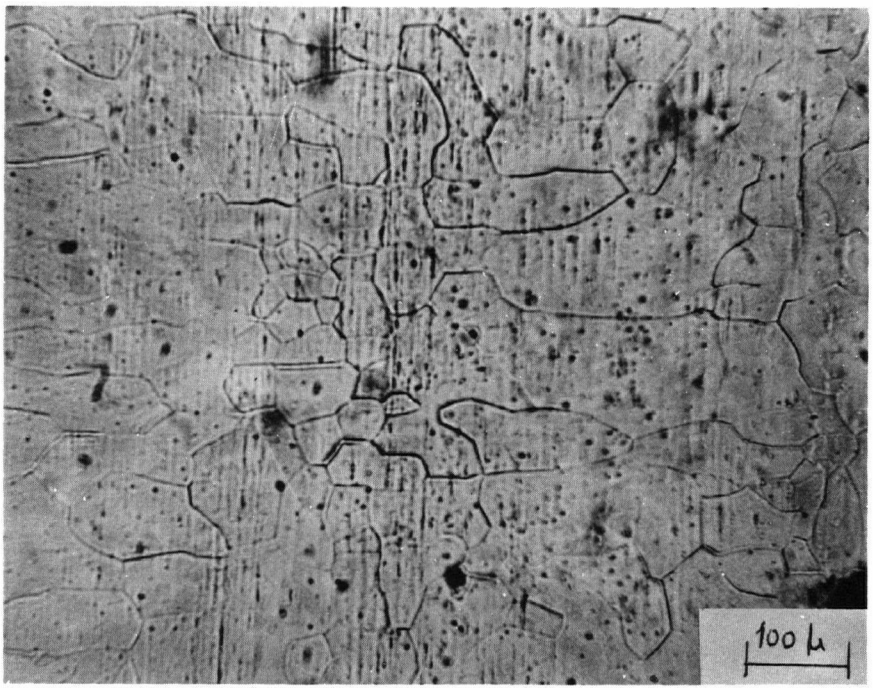

Figure 17. Optical micrograph of 400°C extruded and annealed aluminum.

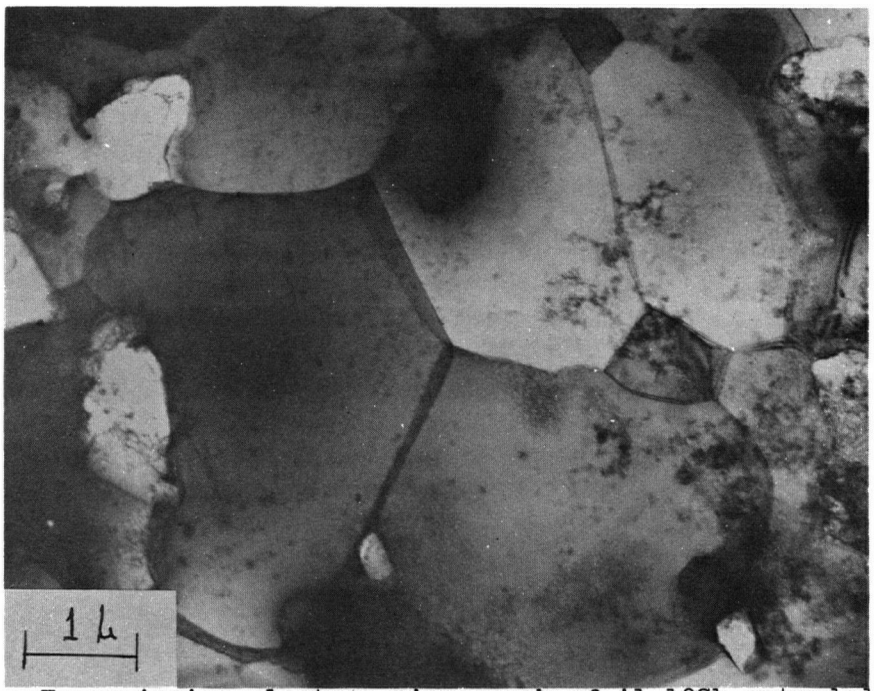

Figure 18. Transmission electron micrograph of Al-10Sb extruded and annealed at 300°C.

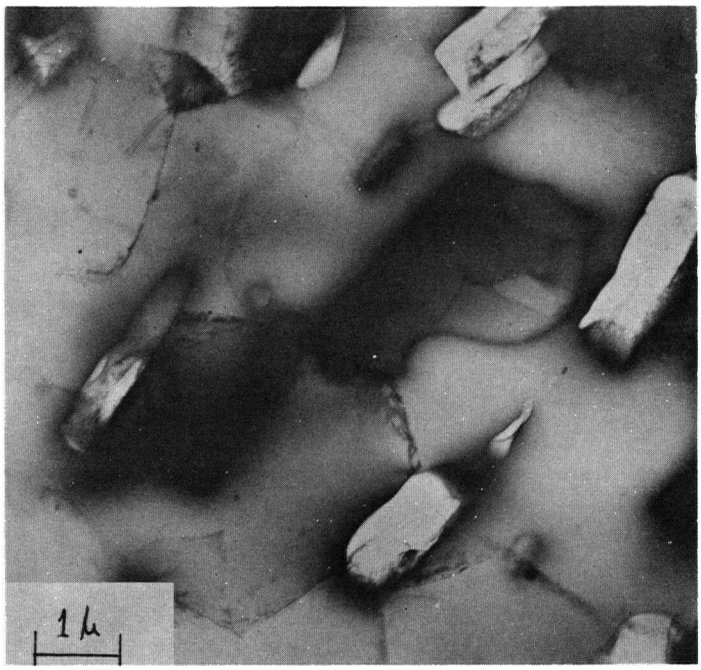

Figure 19. Transmission electron micrograph of Al-10Sb extruded and annealed at 300°C.

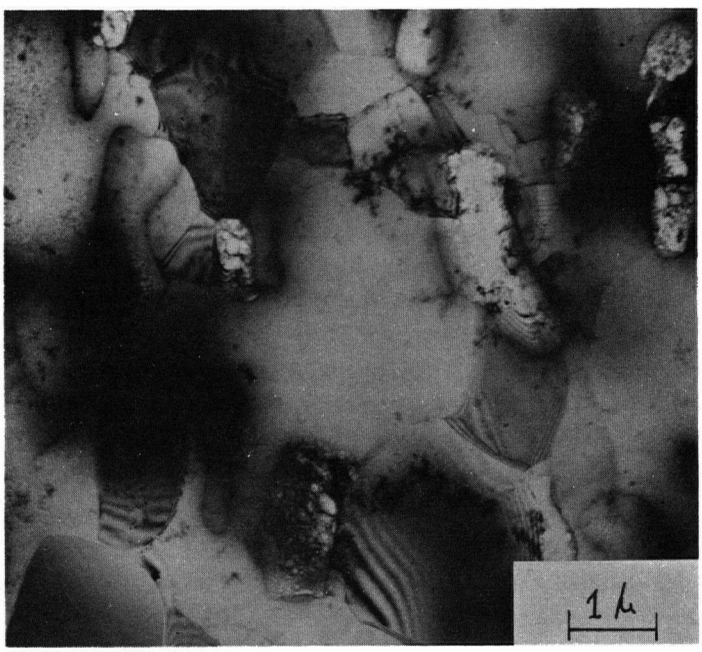

Figure 20. Transmission electron micrograph of Al-10Sb extruded and annealed at 300°C.

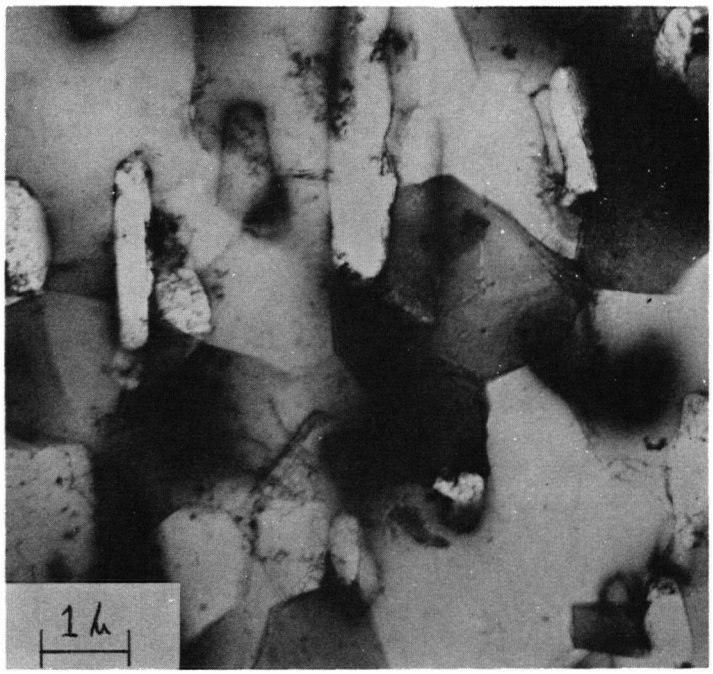

Figure 21. Transmission electron micrograph of Al-10Sb extruded and annealed at 300°C.

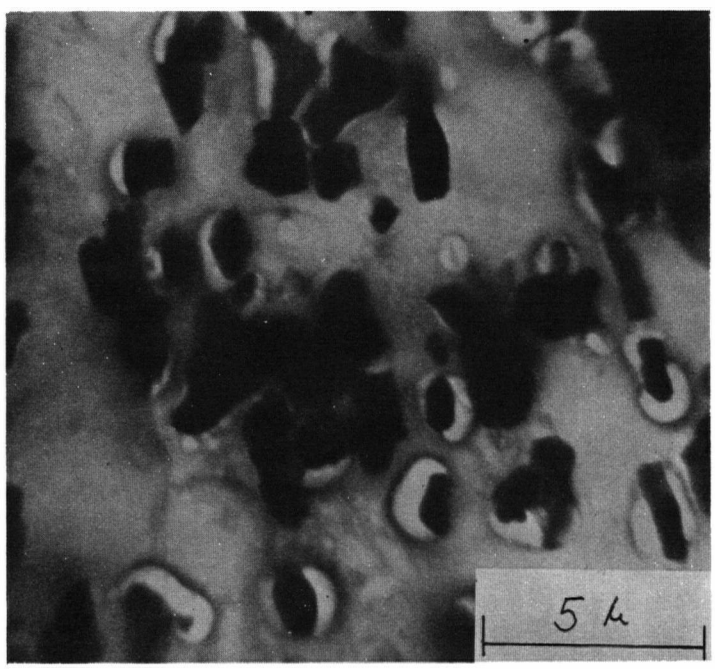

Figure 22. Transmission electron micrograph of Al-10Sb extruded and annealed at 300°C, showing AlSb particles.

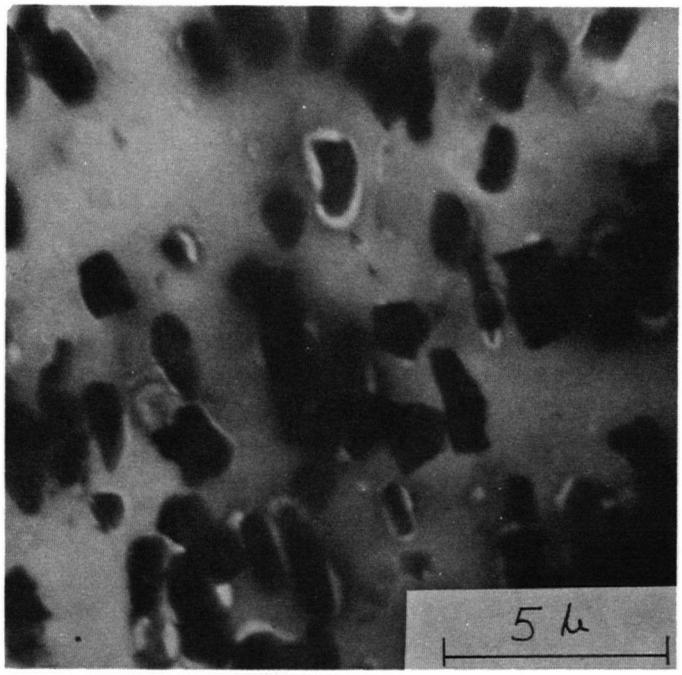

Figure 23. Transmission electron micrograph of Al-10Sb extruded and annealed at 300°C, showing AlSb particles.

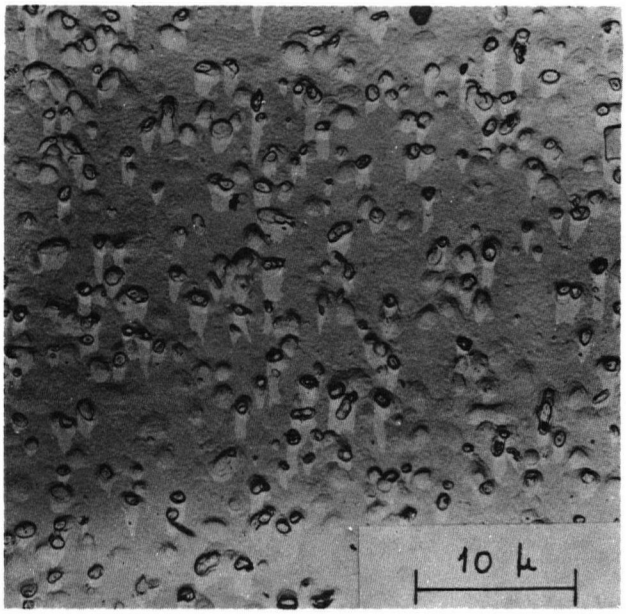

Figure 24. Replica micrograph showing the size of AlSb particles, compared to Figure 25.

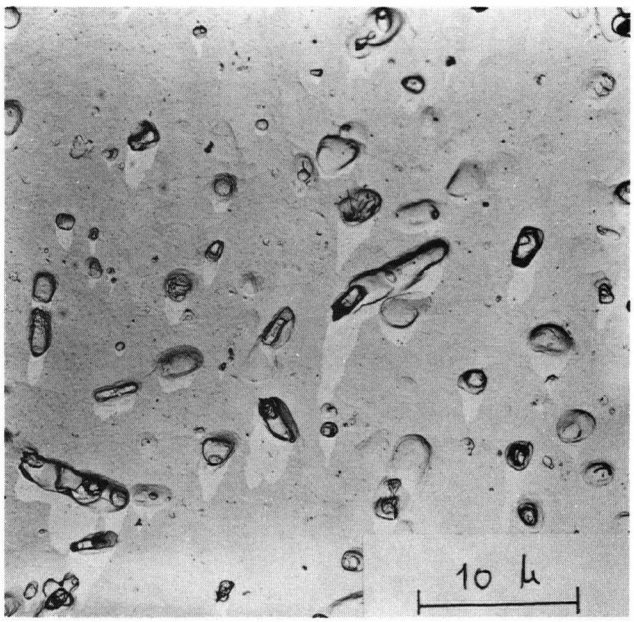

Figure 25. Replica micrograph showing the size of AlSb particles, compared to Figure 24.

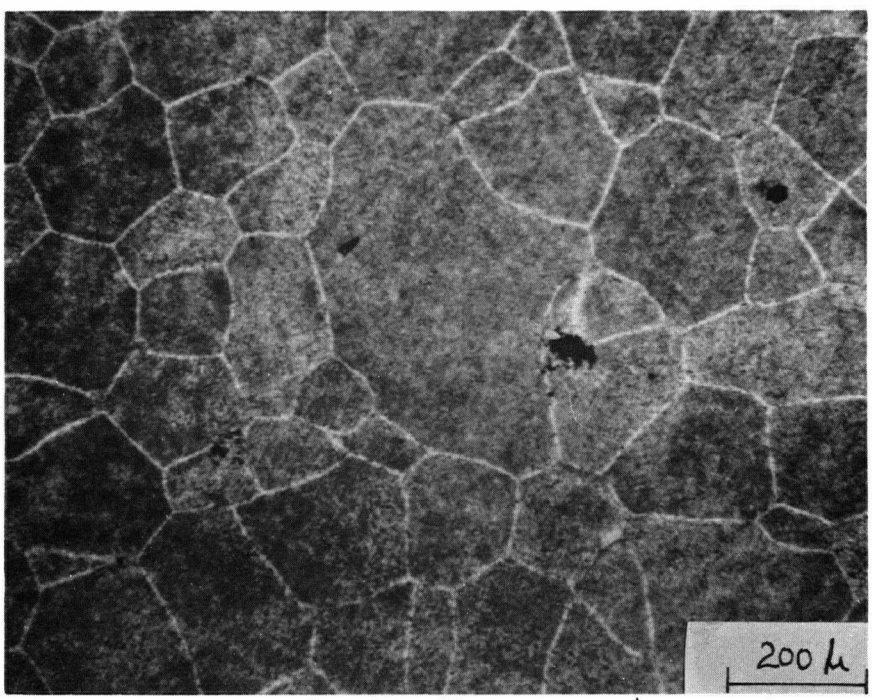

Figure 26. Optical micrograph of overaged Al-4Cu showing grain size.

Aluminum - 4% Copper

Figure 26 is an optical micrograph of the overaged Al-4Cu alloy. The matrix grains are equiaxed and large (220 μ m).

Figure 27 is an enlarged optical micrograph of the alloy which reveals the extremely fine nature of the dispersion of $CuAl_2$ particles in relation to the grain size.

Figure 28 is an optical micrograph of the solution treated Al-4Cu alloy. The grains are equiaxed and coarse (270 μm).

Tensile Data - General

Values of yield stress (0.2% offset), ultimate tensile strength, total percent elongation and percent uniform elongation are collected in Tables 4 through 10 for different strain rates and temperatures, and for all the materials investigated. A yield stress at less than 0.2% offset was not obtainable from the machine curves with adequate reproducibility.

In most of the work two tests were performed under each set of conditions to check the reproducibility of each result. The variation in the strength parameter was generally less than 2% and was less than 5% in all cases. There was more scatter in the results for the elongation parameters, which was not unexpected because of the inherent limitations of such data.

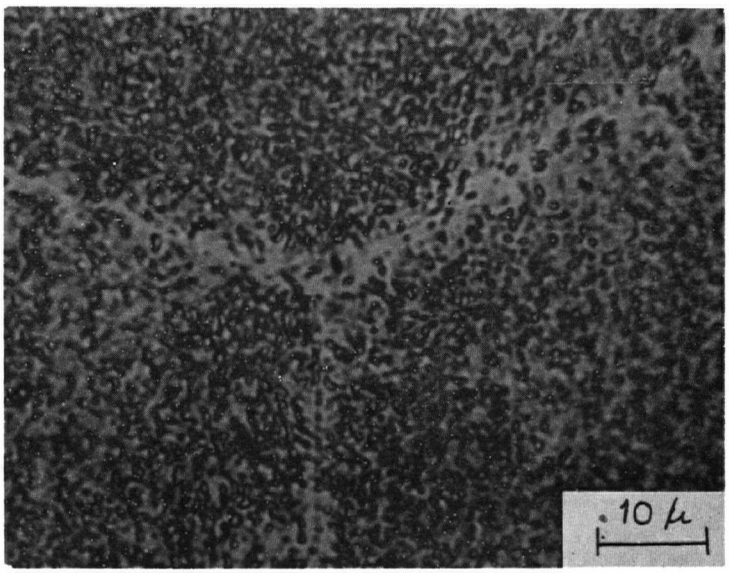

Figure 27. Optical micrograph of overaged Al-4Cu showing fine nature of $CuAl_2$ dispersion in relation to grain size.

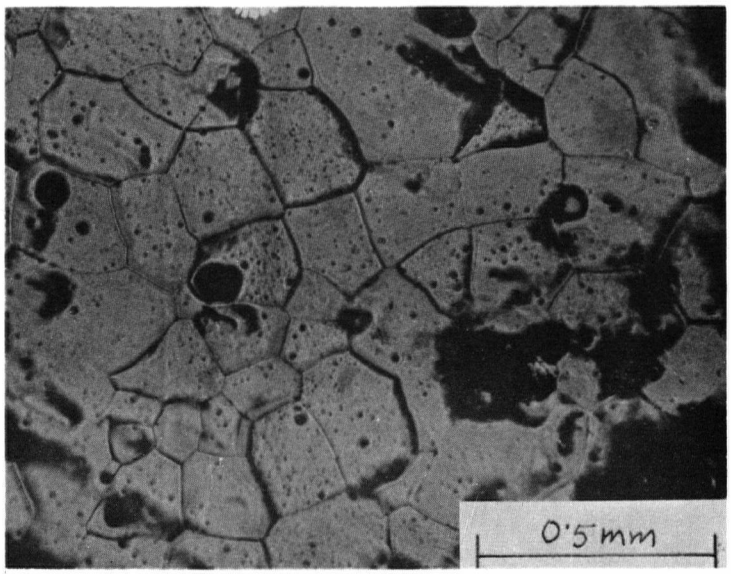

Figure 28. Optical micrograph of solution treated Al-4Cu showing grain size.

Table 4

Tensile Data for 2.7 μm Aluminum

Temperature of Test °C	Strain Rate sec^{-1}	Yield Strength (0.2% offset) p.s.i.	Ultimate Tensile Strength p.s.i.	Total percent Elongation	Uniform percent Elongation
-100	0.33×10^{-3}	14,900	17,000	24	19.2
		15,500	17,000	21	16.7
20	0.33×10^{-4}	13,500	14,100	5.4	1.2
		13,700	13,800	5.6	1.3
	0.33×10^{-3}	14,700	14,800	5.4	1.1
		14,700	14,800	5.8	1.3
	0.33×10^{-2}	14,100	14,100	5.9	1.1
		14,100	14,100	6.8	2.6
100	0.33×10^{-3}	13,000	13,100	6.1	1.1
		12,800	13,200	6.3	1.2
200	0.33×10^{-3}	10,100	10,500	7.9	1.4
		10,300	10,500	7.1	1.3

Table 5

Tensile Data for 3.5 μ m Aluminum

Temperature of Test °C	Strain Rate sec^{-1}	Yield Strength (0.2% offset) p.s.i.	Ultimate Tensile Strength p.s.i.	Total percent Elongation	Uniform percent Elongation
-100	0.33×10^{-3}	15,100	16,900	23.2	15.7
		15,100	17,800	26.6	19.4
20	$0,33 \times 10^{-4}$	13,300	13,300	9.7	2.0
		12,500	12,900	11.1	3,0
	$0,33 \times 10^{-3}$	13,200	13,600	11.8	3.8
		12,900	13,300	14.8	6.6
	0.33×10^{-2}	12,600	13,500	15.2	5.8
		12,500	14,000	17.7	6.9
100	0.33×10^{-3}	12,200	12,400	9.7	1.0
		12,400	12,800	10.2	1.0
200	0.33×10^{-3}	10,500	10,500	10.0	1.1
		9,900	9,900	10.0	1.0

Table 6

Tensile Data for 10 μm Aluminum

Temperature of Test °C	Strain Rate sec^{-1}	Yield Strength (0.2% offset) psi	Ultimate Tensile Strength psi	Total percent Elongation	Uniform percent Elongation
-100	0.33×10^{-3}	9,500	17,000	35.9	25.2
		9,400	15,700	39.5	31.5
20	0.33×10^{-4}	8,600	10,200	27.4	18.4
		10,000	10,900	22.8	13.6
	0.33×10^{-3}	8,600	11,400	31.1	21.1
		9,000	11,100	30.2	21.1
	0.33×10^{-2}	8,000	11,400	31.8	23.8
		8,900	11,300	31.1	22.8
100	0.33×10^{-3}	7,800	8,800	26.6	13.8
		7,900	9,000	26.3	12.8
200	0.33×10^{-3}	6,000	6,000	13.6	1.8
		6,000	6,100	13.6	1.0

Table 7

Tensile Data for 98 μm Aluminum

Temperature of Test °C	Strain Rate sec^{-1}	Yield Strength (0.2% offset) psi	Ultimate Tensile Strength psi	Total percent Elongation	Uniform percent Elongation
-100	0.33×10^{-3}	3,800	-	-	-
20	0.33×10^{-3}	2,800	10,000	41.4	32.6
100	0.33×10^{-3}	2,600	7,800	42.8	28.6
200	0.33×10^{-3}	1,600	4,300	41.9	20.2

Table 8

Tensile Data for Al-10Sb

Temperature of Test °C	Strain Rate sec^{-1}	Yield Strength (0.2% offset) psi	Ultimate Tensile Strength psi	Total percent Elongation	Uniform Percent Elongation
-100	0.33×10^{-3}	16,400	26,200	22.6	17.7
		16,100	26,300	25.0	21.6
20	0.33×10^{-4}	13,400	18,500	23.8	14.0
		14,000	18,800	24.6	14.5
	0.33×10^{-3}	15,100	20,000	23.4	17.1
		15,000	19,700	25.0	19.3
	0.33×10^{-2}	13,900	20,500	21.8	17.4
		14,200	20,300	20.9	15.7
100	0.33×10^{-3}	12,600	15,200	20.6	12.0
		12,900	15,000	21.0	13.1
200	0.33×10^{-3}	10,600	10,700	19.7	1.2
		10,800	10,900	16.3	1.1

Table 9

Tensile Data for Overaged Al-4Cu

Temperature of Test C	Strain Rate Sec^{-1}	Yield Strength (0.2% offset) psi	Ultimate Tensile Strength psi	Total percent Elongation	Uniform percent Elongation
-100	$0.33x10^{-3}$	15,600	34,000	11.7	10.4
		15,400	36,000	12.2	11.2
20	$0.33x10^{-4}$	14,600	35,100	11.3	10.5
	$0.33x10^{-3}$	16,600	36,800	11.5	9.6
		16,200	36,100	11.8	10.4
	$0.33x10^{-2}$	16,800	36,300	9.8	8.1
100	$0.33x10^{-3}$	15,400	31,200	12.5	7.9
200	$0.33x10^{-3}$	13,400	19,400	11.3	6.2

Table 10

Tensile Data for Solution Treated Al-4Cu

Temperature of Test C	Strain Rate sec^{-1}	Yield Strength (0.2% offset) psi	Ultimate Tensile Strength psi	Total percent Elongation	Uniform percent Elongation
20	$0.33x10^{-3}$	21,800	39,400	21.7	18.5

Because of the relatively good reproducibility observed in the strength results for the other materials only one test was performed under each set of conditions for 98 μm pure aluminum and in some instances for Al-4Cu.

Tests at different strain rates were not performed on the 98 μm aluminum as the results obtained earlier with pure aluminum did not suggest enough dependence on strain rate at room temperature to justify a continuation of the practice.

It was not possible to obtain the ultimate tensile strength and elongation values in the case of 98 μm Al at -100°C because of the practical difficulty of avoiding grip-slippage with this material.

Yield Stress of Polycrystalline Aluminum

Figure 29 shows the variation of 0.2% offset yield stress for aluminum with test temperature.

Carreker et al[20] have investigated the tensile behaviour of two sets of polycrystalline aluminum which had the following analysis:

(AC) Si 0.006%, Cu 0.015%, Fe 0.006%, Al 99.975%

(BS) Si 0.006%, Cu 0.002%, Fe0.003%, Al 99.987%

Lot BS was reported to show no grain size dependence of yield strength, although there was considerable scatter in the data. Reported results for lot AC are reproduced in Figure 29 for comparison with the present results. The range of grain size studied by Carreker et al[20]

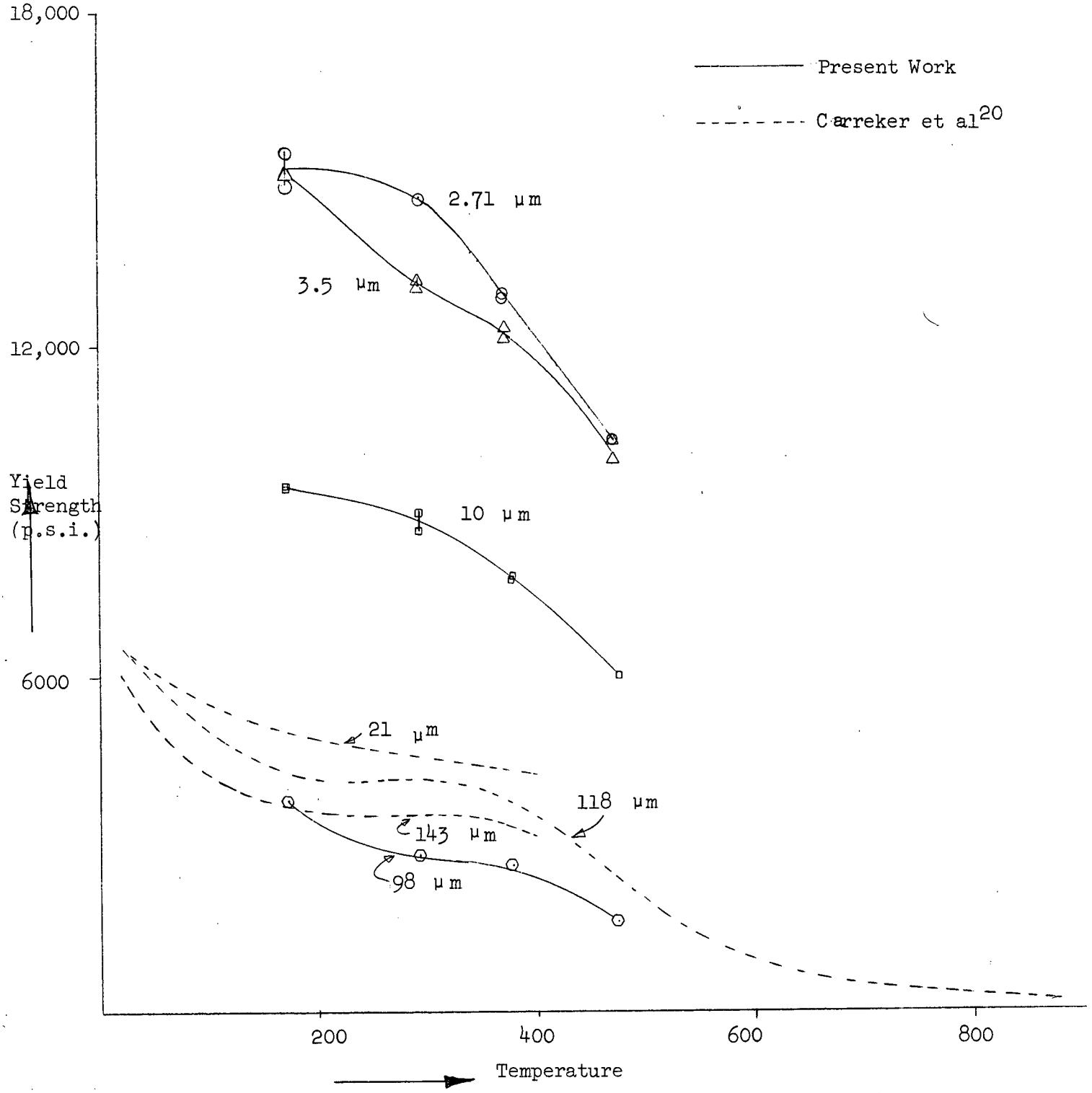

Figure 29. Variation of Yield Strength with Temperature for Different Grain Sized Aluminum

was limited, their finest material having 21 μm grains.

For comparable grain sizes Carreker et al have observed a higher yield stress value than in the present work. This was not unexpected because the flow stresses in the former work were measured at 0.5% offset as opposed to the 0.2% offset used in the present work.

The most important finding of the present work in this regard is the marked increase in the yield strength of pure polycrystalline Al, as a result of refinement in the grain size, at all the temperatures investigated within the range 0.19 Tm to 0.51 Tm.

Figure 30 shows a plot of yield stress (0.2% offset) against $l^{-1/2}$ where l is the initial grain size or sub grain size, for pure aluminum at the four test temperatures.

Ultimate Tensile Strength

Figure 31 is a plot of ultimate tensile strength as a function of temperature for all the materials investigated.

The finer the grain size, the higher was the U.T.S. for pure aluminum at all temperatures. A gradual decrease can be seen in the U.T.S. values for pure aluminum with increasing temperature for all grain sizes.

The U.T.S. of Al-10Sb was higher than that of pure aluminum of comparable grain size over the entire temperature range investigated. The difference was more marked at lower temperatures.

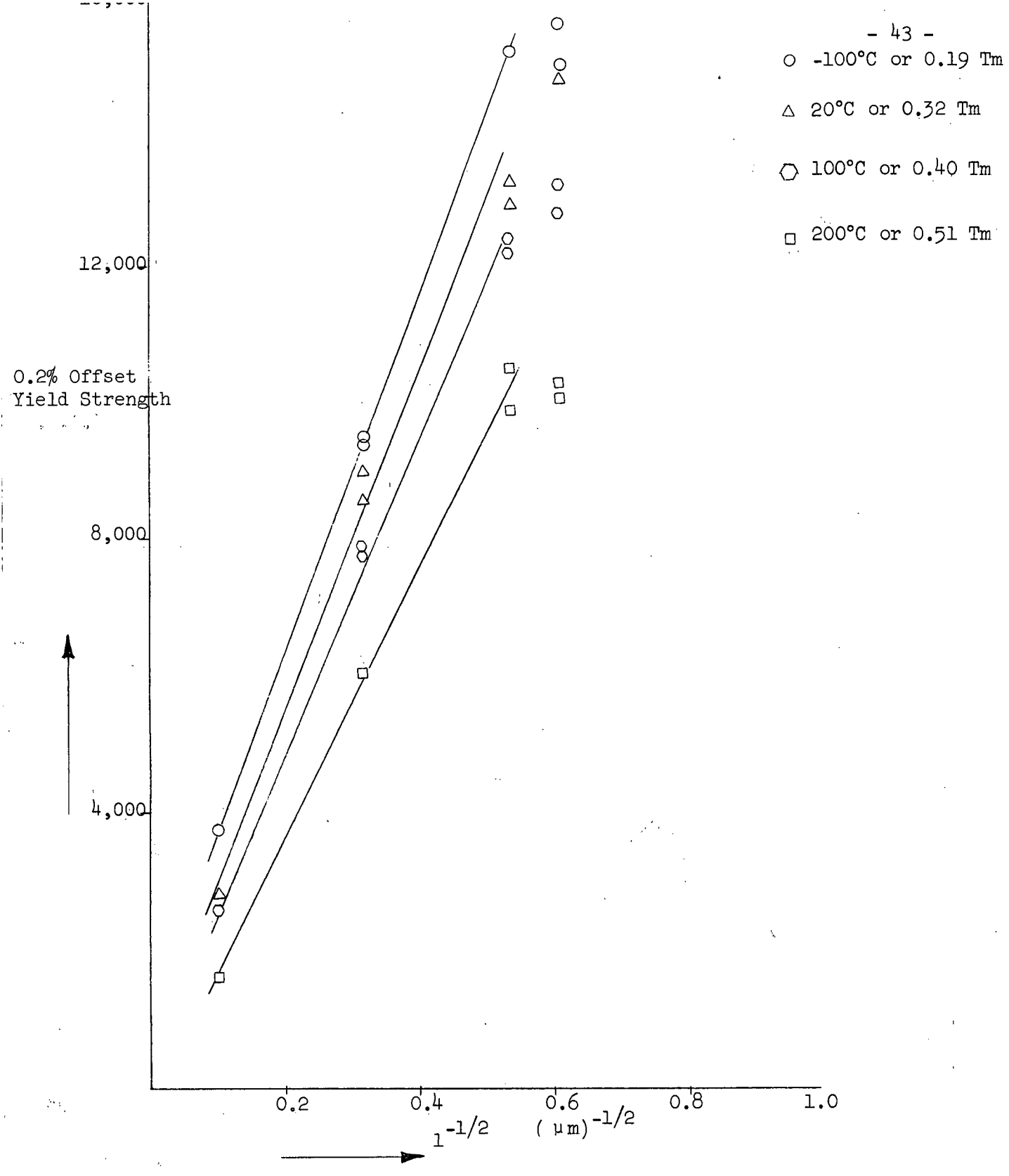

Figure 30. Yield Strength V/S (grain size)$^{-1/2}$ For Aluminum at Different Test Temperatures.

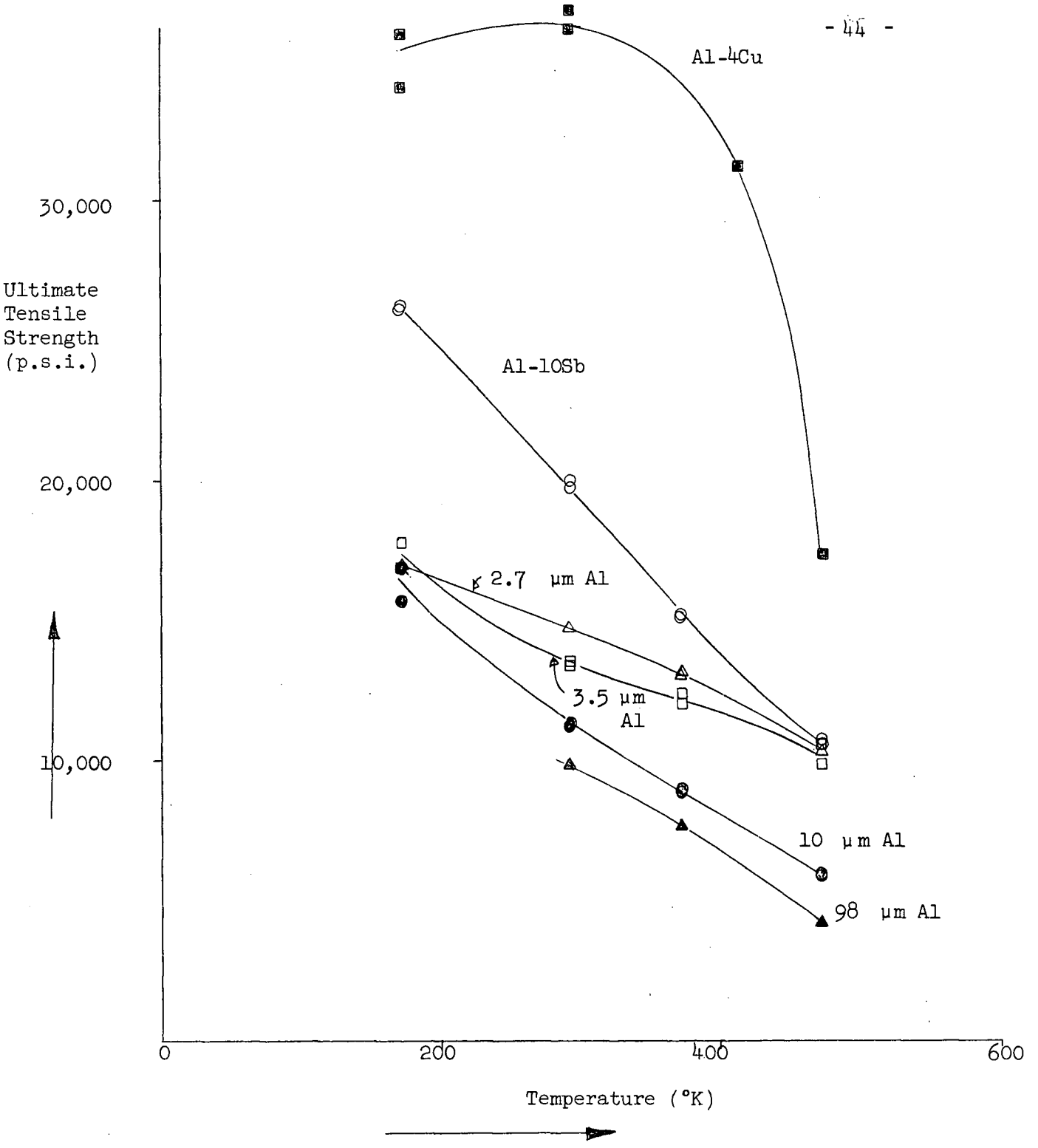

Figure 31. Variation of Ultimate Tensile Strength with Temperature For Aluminum and Alloys

A relatively rapid drop in the U.T.S. of overaged Al-4Cu at 200°C was observed.

Percent Elongation

Because of the marked dependence of total elongation (to fracture) on such factors as specimen geometry and gauge length, it is not meaningful to compare present values with others previously reported for aluminum. The amount of uniform elongation (i.e. prior to local necking) is generally a more useful parameter although it is found to be difficult to assess this quantity if the machine curve does not show a well-defined peak.

Percent uniform elongation is plotted as a function of temperature, for all the materials investigated, in Figure 32. An increase in the value of total elongation with decreasing temperature below 300°K was reported by Carreker et al[20]. Similar behaviour is observed with respect to total elongation as well as uniform elongation in the present work.

All the finer grained materials appeared to reach a limiting lower value of percent uniform elongation with rising temperature. This was reached for 2.7 μm aluminum at room temperature, for 3.5 μm aluminum at 100°C and for 10 μm aluminum at 200°C. Al-10% Sb, which maintained its ductility with increasing temperature compared with pure aluminum of comparable grain size, did reach the lower limiting value at 200°C.

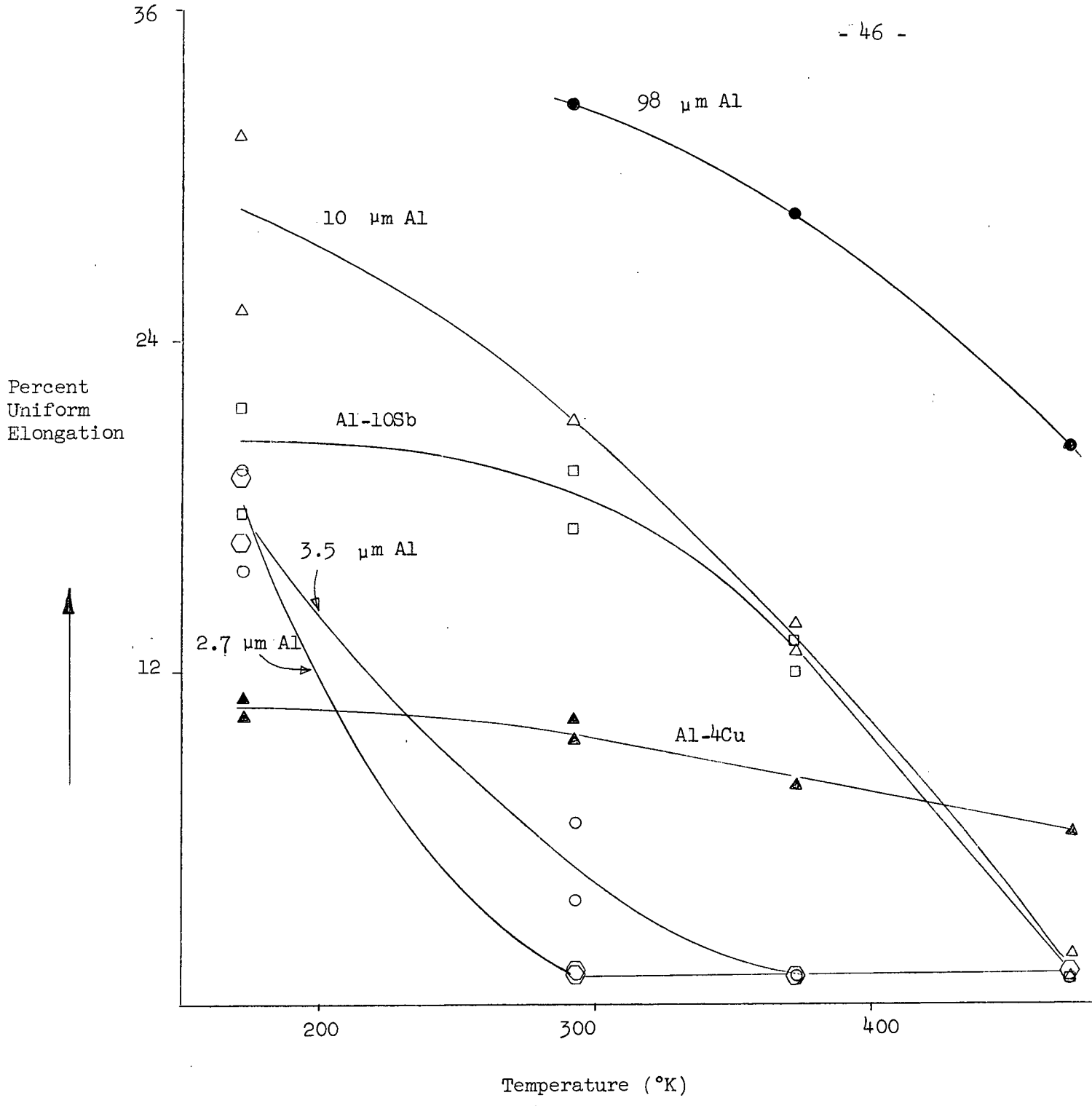

Figure 32. Variation of Percent Uniform Elongation with Temperature for Aluminum and Alloys

Overaged Al-4Cu loses ductility with increasing temperature at an appreciably lower rate than any other of the materials investigated in the temperature range of 0.2 to 0.5 Tm. Pure aluminum of 98 μm grain size is more ductile than any of the other materials over the temperature range investigated, but it loses its ductility at higher temperatures faster than the overaged Al-4Cu alloy.

Work Hardening Rates

During homogeneous plastic deformation in tension, the true stress σ and true strain ε are often found to be empirically related by an expression of the form

$$\sigma = K \varepsilon^{n}$$

where n is defined as the strain hardening exponent, and

K is the strength coefficient

It should be noted that there is nothing basic about the relationship, and its validity is open to question. However, the equation has been found by many other investigators to be useful in comparing the work hardening rates of different materials. In many cases n has been found to change with strain, and comparisons are possible only within those limited ranges of strain where n may be reasonably assumed to be constant.

For the present work $\log \sigma$ has been plotted against $\log \varepsilon$. In most cases the value of n was found to change gradually over the complete strain region. However, an attempt was made to compare average values of n over the small plastic range of 0.2% to 2% (Table 11).

Table 11

Table of Work Hardening Exponent (n)

Material	Value of $n_{(epl\ .002 - 0.02)}$ at			
	-100°C (0.19Tm)	20°C (0.32Tm)	100°C (0.40Tm)	200°C (0.51Tm)
2.7 μm Al	0.028	*	*	*
3.5 μm Al	0.021	0.028	*	*
98 μm Al	0.29	0.35	0.30	0.33
2.9 μm Al-10Sb	0.14	0.079	0.064	*
Overaged Al-4Cu	0.28	0.30	0.30	0.18
Solution Treated Al-4Cu	-	0.13	-	-

* Material necks down at very low strains

\- No test was performed

It was not possible to estimate n values for the 10 μm aluminum specimens because of the discontinuous yielding behaviour this material exhibited in the strain range of interest. Fine grained materials necked after very small strains at higher temperatures and no value of n was reported for these cases.

From Table 11 the following observations can be made about the work hardening rates of various materials in the strain range 0.2 to 2%.

(1) The two finest grained aluminum extrusions showed a very low rate of work hardening at temperatures where work hardening could be observed at all.

(2) The fine grained Al-10Sb alloy work hardened much more rapidly at 0.19 Tm than at 0.32 Tm or 0.40 Tm.

(3) The coarsest grained aluminum and overaged Al-4Cu exhibited a comparatively high rate of work hardening at all temperatures, although the value of n for Al-4Cu dropped appreciably at 0.51 Tm.

(4) Solution treated and quenched Al-4Cu had a substantially lower work hardening rate than overaged Al-4Cu at room temperature.

Discontinuous Yielding

An incidental observation during this work was that a number of drops in stress occurred during the earlier stages of deformation of aluminum which had been annealed at 300°C and which had a grain size of 10 microns.

The phenomenon was never observed in aluminum specimens that were annealed at 200°C or 400°C. For the 300°C annealed aluminum, the phenomenon was observed at all the three strain rates (0.33×10^{-4}, 0.33×10^{-3}, 0.33×10^{-2} sec^{-1}) investigated at room temperature and at all the test temperatures where there was any work-hardening at all, namely -100°C, 20°C and 100°C.

The relevant portion of a load-elongation curve showing the load drops in 300°C extrusions tested at 20°C and 0.33×10^{-3} sec^{-1} is reproduced in Figure 33. The drops in all cases were distinct. Five such drops could be seen in Figure 33.

The number of drops varied from 3 to 5 in the range of strain rate and temperature investigated. A marked regularity was noted regarding drops D_4 and D_5 which also were detected in all the tests. The strains at which these last two drops occurred are collected in Table 12.

A trend toward increasing values of the plastic strain at which drops D_4 and D_5 occur with increasing temperature or decreasing strain rate can be seen in Table 12.

Carreker et al[20], also reported that they observed a yield phenomenon at test temperatures below 195°K in pure polycrystalline aluminum which was annealed at 300°C and had a grain size of 21 microns. They have reported its absence in aluminum annealed at 400°C and 500°C. However, no details of the load drops were documented.

Present work establishes the absence of this phenomenon in aluminum annealed at 200°C.

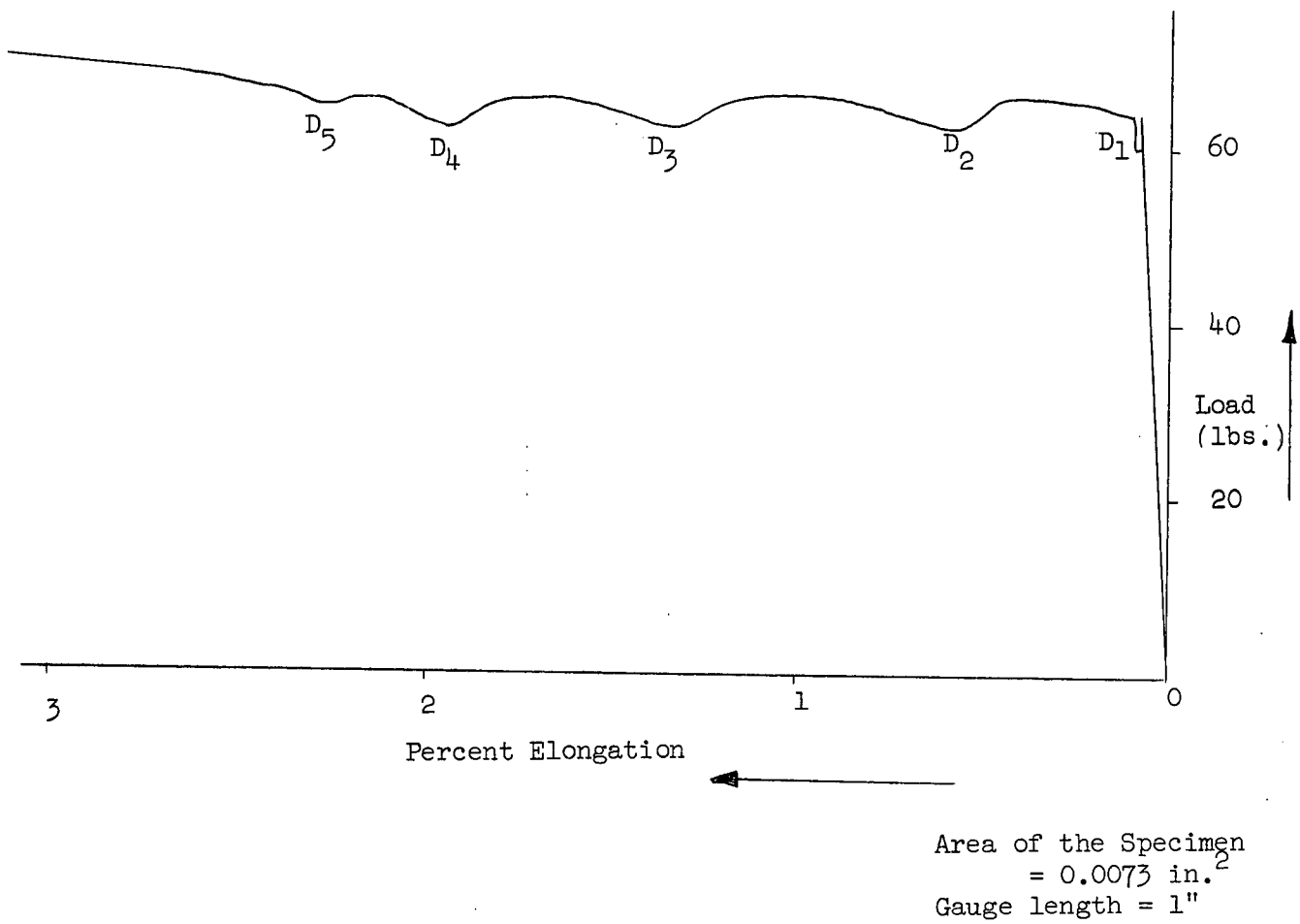

Figure 33. Discontinuous Yielding

Table 12

Tabulation of Plastic Strains at Which Drops D_4 and D_5 Occur

Temperature of Test °C	Strain Rate sec^{-1}	Plastic Strain Value For D_4 Percent	Plastic Strain Value For D_5 Percent
-100	0.33×10^{-3}	1.2	1.3
		1.1	1.3
20	0.33×10^{-4}	1.5	2.6
		2.8	4.0
	0.33×10^{-3}	2.0	2.5
		1.6	2.1
	0.33×10^{-2}	0.6	1.7
		1.3	1.7
100	0.33×10^{-3}	2.1	2.5
		3.5	4.5
200	0.33×10^{-3}	-	-
		-	-

A Pure Aluminum

(a) Deformation Behaviour

Heiderreich[21], using a transmission electron microscopy technique, showed that the grains of high purity polycrystalline aluminum are broken up during deformation into units which he described as an arrangement of slightly misoriented "crystal domains" (now called "cells").

A series of X-ray investigations by Gay et al [22-25] showed that a cell structure is present in other deformed face-centered cubic metals (copper, nickel, lead) as well as in aluminum and some body centered cubic metals. They concluded that the cell size is independent of the initial grain size and decreases to a limiting value after a certain strain.

These results have since been confirmed by transmission electron microscopy of thin metal foils[26]. The cells were found to be relatively free of dislocations but were separated by walls of high dislocation density.

Weissmann et al[19], have studied the details of the dislocation structure of cold worked high-purity polycrystalline aluminum and the processes which occur in recrystallisation. They have suggested that the dislocation tangles (which represent the initial stage of formation of a dislocation cell structure) are formed as a result of the mutual attraction of dislocations in primary and secondary slip systems. They found that increasing deformation gives rise to a cell structure which exhibits well-delineated dislocation boundaries after about 30% reduction. Additional cold working increased the dislocation density as well as the twist and asymmetry of the low-angle boundaries separating the cells. No appreciable increase in dislocation density within the cells was found, nor was any decrease in cell size observed

with further cold working. The increase in dislocation density within the cell walls with increasing deformation was explained as resulting from the attraction which screw dislocations in the cell walls exert on dislocations generated within the cell. It was suggested that the formation of dense tangles in the cell walls was facilitated by the ease with which dislocations can circumvent obstacles within the cell by means of cross-slip.

Weissmann et al[19] further suggest that there is an interconnection between the mechanical and thermal instability of asymmetrical low angle boundaries. The strengthening effect of the low angle boundaries was attributed to the effective stress field of screw dislocations, which are mechanically stabilised by the edge dislocations. The stress field of the screw dislocations was also considered to be responsible for the thermal instability of the low-angle boundaries, which on annealing are gradually converted into pure tilt boundaries.

(b) Structure of 200°C Extruded and Annealed Aluminum

Structural changes taking place in aluminum as a result of heavy deformation (extrusion ratio of 25 to 1) at 200°C are likely to be the result of cooperative processes. Cell structure formation (expected due to deformation) probably competed with simultaneous recovery processes. However, because the deformation involved was at a very high rate, a cell structure more typical of cold deformed aluminum probably formed.

Subsequent annealing at 200°C has resulted in the microstructures seen in Figures 5 through 12. Weissmann et al[19], pointed out that screw dislocations are responsible for the thermal instability of asymmetrical low angle boundaries, which on annealing are gradually converted into pure tilt boundaries. He observed that upon annealing it is the screw dislocations

which are first expelled from asymmetrical boundaries (and distorted lattice domains.) The appearance of a characteristic profusion of individual jogged dislocations (as at B in Figure 6) are termed by Weissmann et al[19] as "disentanglement of dislocations." Sharp boundaries (as at A in Figures 5 through 12) are supposed to be principally tilt boundaries, and the resulting structure is termed subgrains.[19]

(c) Tensile Behaviour of Polycrystalline Aluminum

(i) Maximum True Stress

True stress-true strain (plastic only) curves for all the materials tested at four different temperatures are plotted in Figures 34 through 37.

In Figure 34, it can be seen that at -100°C all the pure polycrystalline aluminum extrusions work hardened at different rates, yet reached essentially the same peak value of true stress (where necking commenced). The same observation could be made for all these extrusions in the case of 20°C deformation (Figure 35) except that the finest grained (2.7 μm) extrusions necked after very small strain, and supported a slightly higher maximum true stress than the others. At 100°C (Figure 36) ~~2.5~~ 3.5 μm extrusions also started to neck after little strain. The two coarsest grained extrusions supported nearly the same level of true stress before necking commenced, although the 10 μm aluminum did support slightly more stress than the 98 μm aluminum. At 200°C (Figure 37) there was a substantial dependence of the maximum attained true stress on grain size, although it should be noted that only the coarsest grained extrusion deformed extensively before starting to neck.

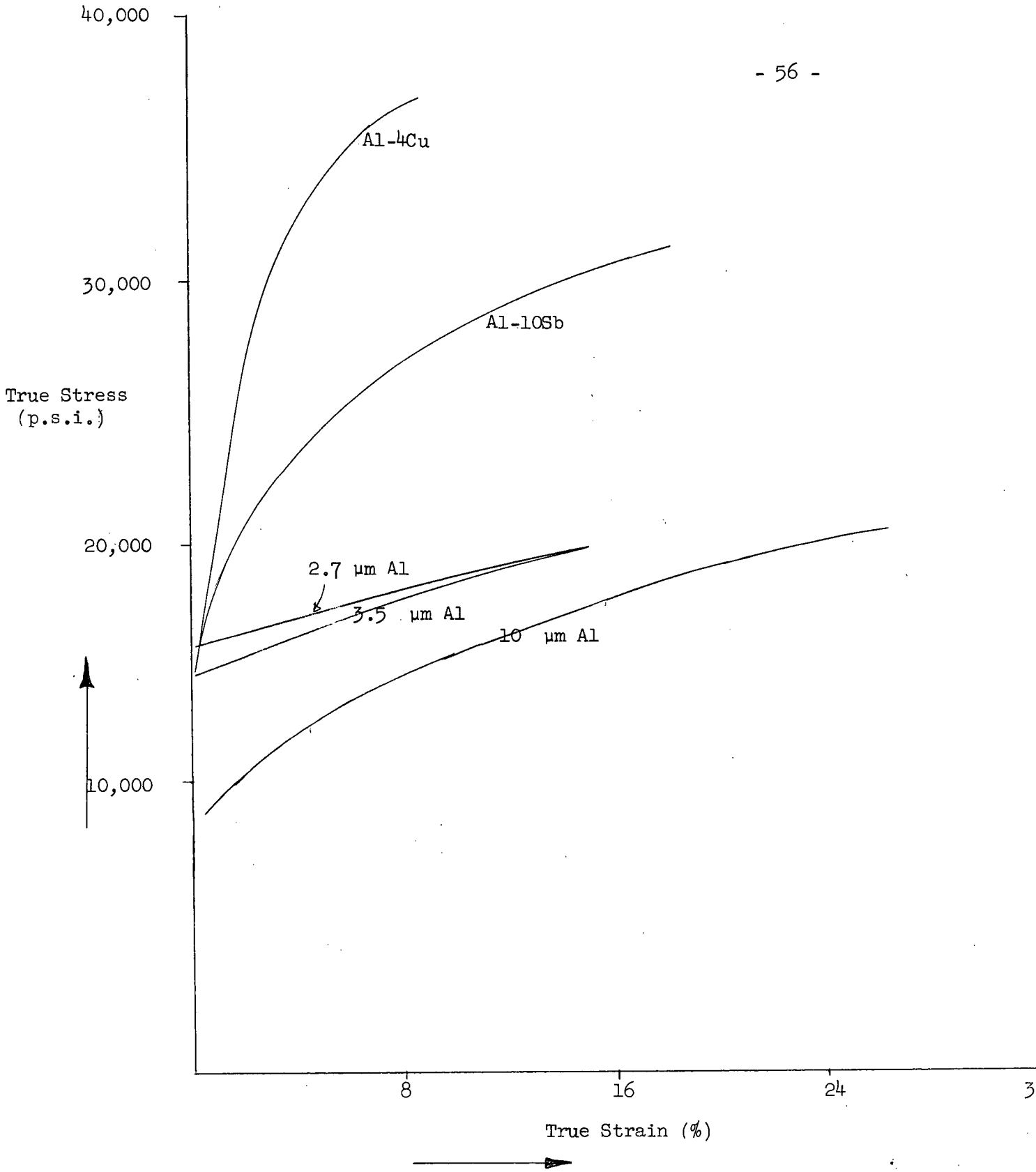

Figure 34. True Stress-Strain Curves for Aluminum and Alloys at -100°C (0.19 Tm)

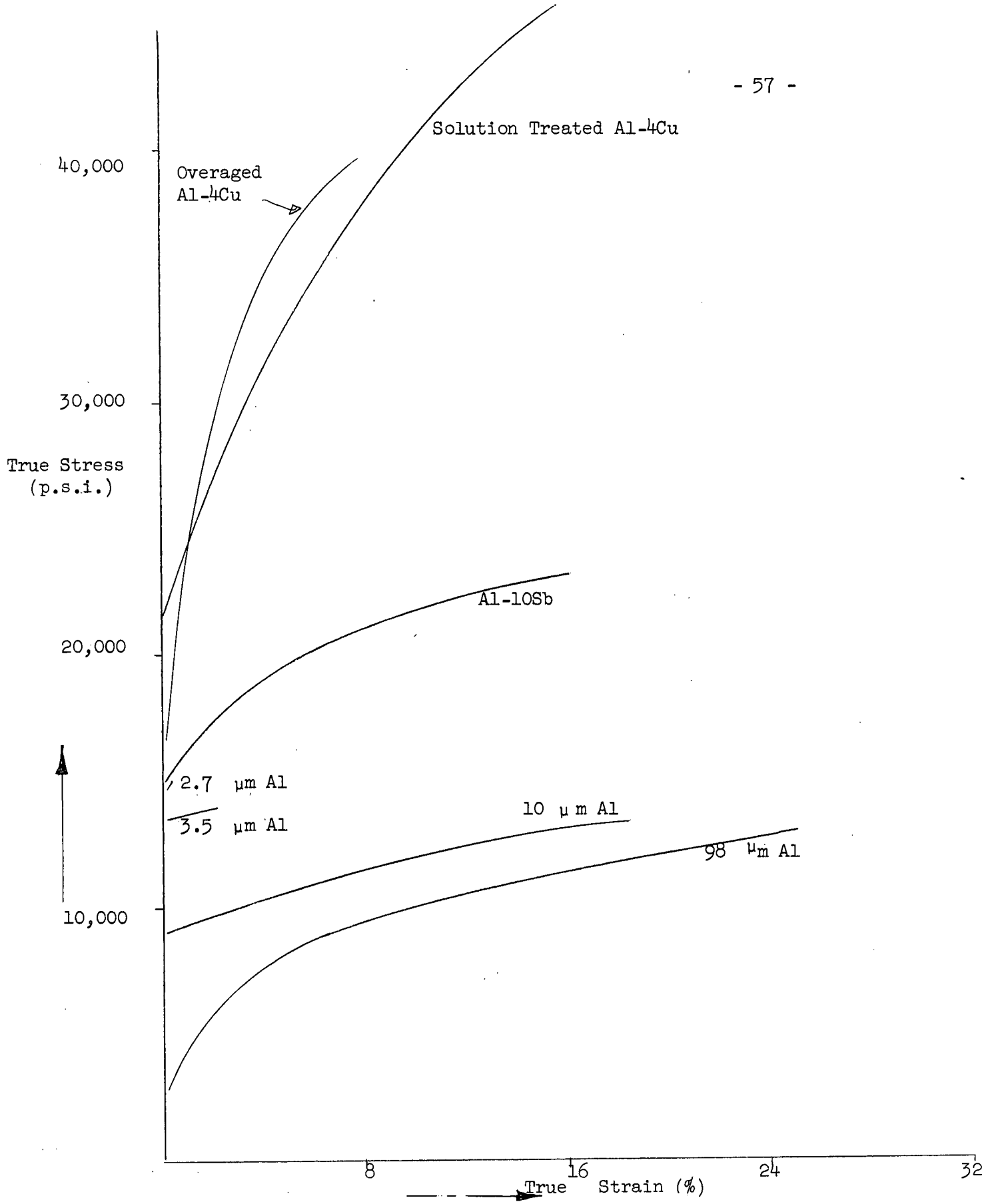

Figure 35. True stress-strain Curves for Aluminum and Alloys at 20°C (0.32 Tm)

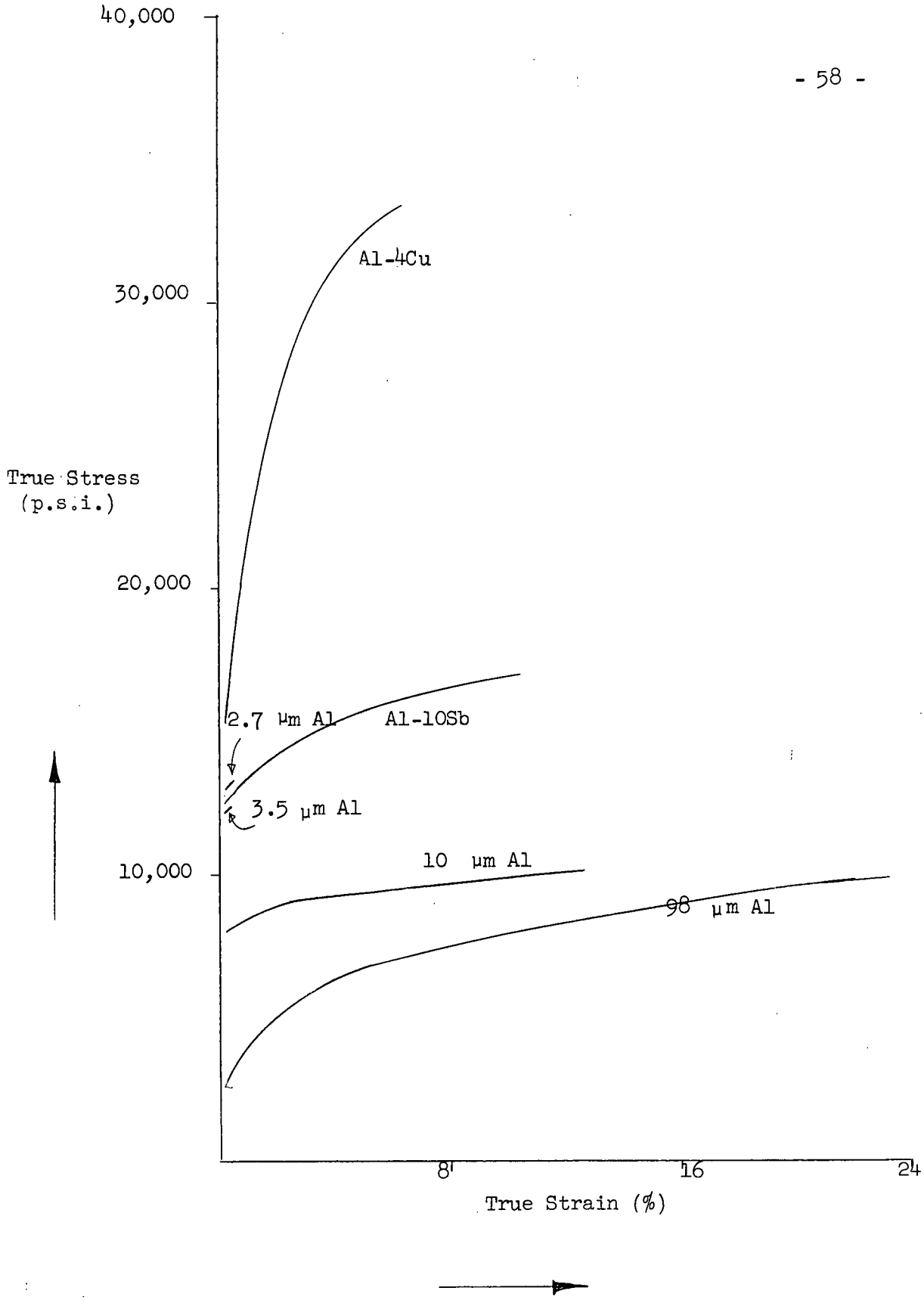

Figure 36. True stress-strain Curves for Aluminum and Alloys at 100°C (0.40 Tm)

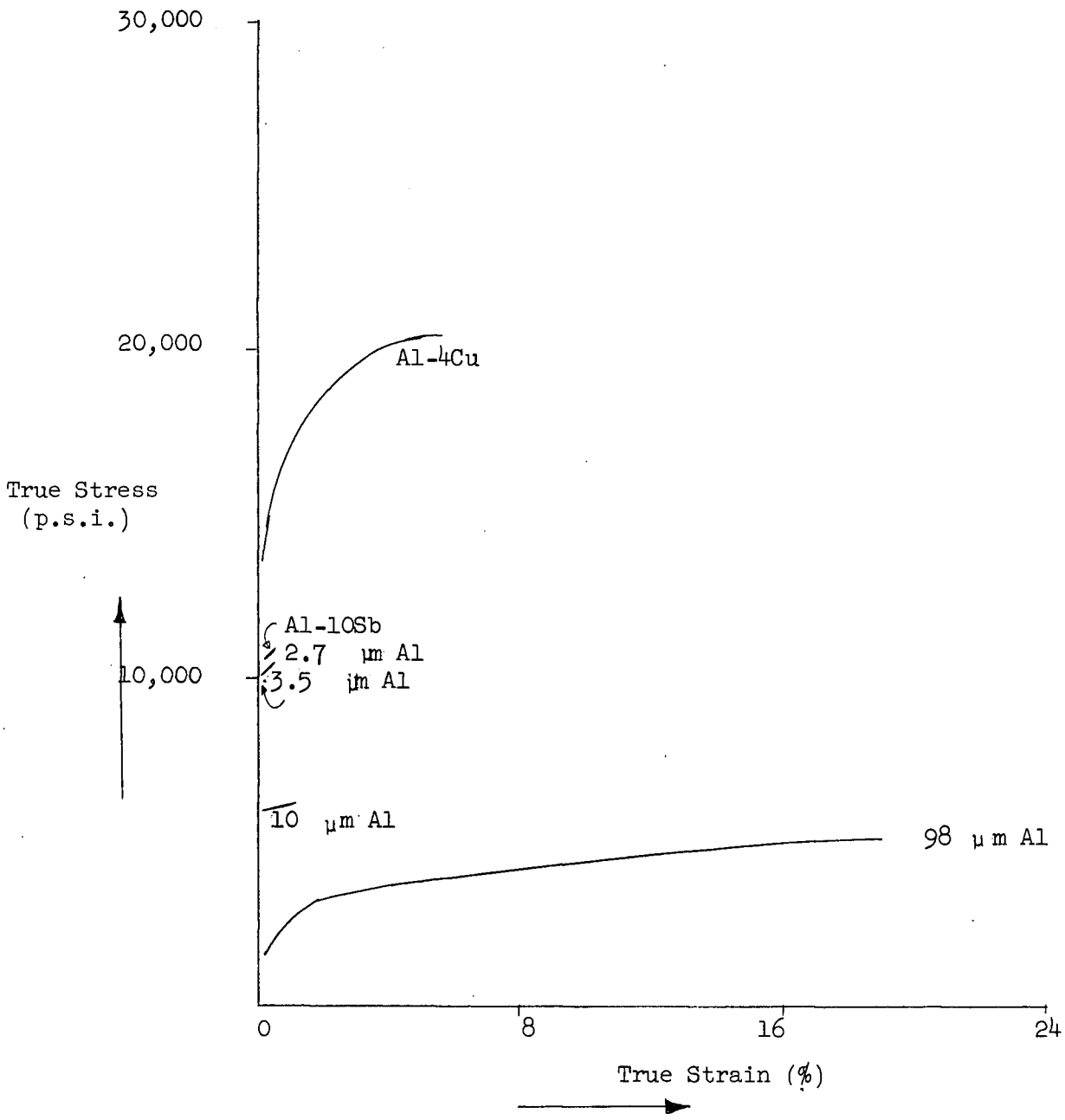

Figure 37. True stress-strain Curves for Aluminum and Alloys at 200°C (0.51 Tm)

The fact that the onset of necking was stress-dependent and apparantly grain size-independent at low temperatures may be explained partially on the basis of a cell formation agruement. The suggestion is that no matter what the starting grain size, if sufficient uniform deformation occurred, a limiting cell size would be attained. Since flow stress is dependent on cell size[25], the flow stress would rise to a value determined by the limiting cell size, and not determined by the original grain size.

Warrington[28] has found that the limiting cell size of copper decreases with decreasing deformation temperature. Typical values reported for copper were 0.6 μm at 0.06 Tm and 7 μm at 0.68 Tm. It has also been found that the limiting cell size for aluminum is decreased by deforming at temperatures below room temperature[27]. Therefore, an increase in the limiting cell size of aluminum can be expected by deforming at temperatures above room temperature as is the case with copper.

At -100°C all the pure aluminum extrusions attain the minimum cell size for this temperature after straining different amounts. At room temperature, it may be argued that the 2.7 μm aluminum has an initial cell size approaching the lower limiting size for 20°C. After very small strains the cell size reaches the minimum and plastic instability sets in because the material no longer work hardens with increasing strain. In fact, the provision of additional strain energy probably promotes the migration of cell boundaries (growth of subgrain boundaries from cells) to produce a form of "work-softening." This argument is equivalent to one which says that recovery processes are capable of occurring locally in aluminum at 20°C in regions of very high strain energy.

Similarly the 3.5 μm extrusion at 20°C work hardens as fast as smaller cells are produced. Because of the small initial subgrain size, the minimum cell size for 20°C is reached after only 2% strain (Figure 35). By contrast, the coarser grained extrusions undergo considerably more strain before the minimum cell size is attained for 20°C. Also, the maximum true stress reached decreases slightly with increasing grain size. This probably results from the fact that thermally activated processes contribute to recovery, and that more time is available for such processes to operate while the initially coarse grained extrusions are deformed. Thus competition between strain-activated cell-wall migration may result in the limiting cell size (and maximum true stress) being slightly grain-size dependent at 20°C.

Reference to Tables 4 through 6 indicates an increasing value of percent uniform elongation with increasing strain rate. This may be attributed to an increasing amount of dynamic recovery or cell wall migration with decreasing strain rate (i.e. increasing time available for recovery).

At 100°C, the arguments of the previous paragraphs are probably sufficient to account for the observed tensile behaviour of pure aluminum in Figure 36. The relative lack of dynamic recovery in the finest-grained extrusions, and the occurence of it in the coarser grained extrusions can be used to account for the substantially higher value of maximum true stress attained in the former materials.

At 200°C, the large dependence of maximum true stress on initial grain or subgrain size may again be attributed to the effects of dynamic recovery processes on cell formation and growth.

The contribution of grain boundary sliding is known to be greater at higher temperatures. However, its contribution to total deformation in the present work is not likely to be more than 10% at 200°C for any of the materials under investigation[29].

(ii) Work Hardening Behaviour

An explanation of the dependence of work hardening rate on grain size and temperature follows logically from the arguments used above to interpret maximum true stress values.

The effect of increasing strain on cell structure has been studied by Kelly[25] using an X-ray technique. It was found that the cell size is diminished sharply at first and the rate of decrease becomes smaller as the limiting cell size is approached. The result has been confirmed by Swann[27] using transmission electron microscopy.

Accordingly, one sees from Figures 34 through 37 that aluminum extrusions work harden more rapidly in the earlier stages of deformation.

Reference to Table 11 and Figures 34 through 37 reveals that in the present work the rate of work hardening increased with increasing initial grain size. With fine initial grains or subgrains little additional refinement of the substructure results from deformation, and so work hardening from this source is small. The reverse is true for coarse initial grains.

(iii) Yield Stress (0.2% Offset)

The offset yield stress data for pure aluminum extrusions were presented graphically in Figure 30 as plots of $\sigma_{0.2\%}$ v.s. $l^{-1/2}$ where l

is the initial grain or subgrain size. With the exception of results for the extrusions of finest initial grain size, the data appear to obey a Hall-Petch type of relationship at each of the test temperatures. However, it is felt that the apparant linearity of the plots for 3.5 μm to 98 μm extrusions is fortuitous, rather than meaningful, especially at temperatures above -100°C. After 0.2% strain, appreciable microstructural changes have occurred in these materials, depending on test temperature and initial grain size. Thus coarse grained extrusions have work hardened considerably within the first 0.2% strain, whereas fine-grained extrusions have not. At the higher temperatures, even dynamic recovery processes may be influencing the flow stress at 0.2% strain. Thus, in terms of the original arguments[30,31] upon which the Hall-Petch relationship was based, it is unlikely that it can be meaningfully applied to the present offset yield stress results for pure aluminum.

(iv) Percent Uniform Elongation

During work hardening the cell size of a deforming specimen gets finer and finer, and necking sets in when the limiting cell size is reached for the particular test temperature. This attainment of limiting cell size would happen after less deformation if the difference between the initial grain size and final cell size is less. Therefore, a coarse grained extrusion is expected to have a higher value of percent uniform elongation than the finer grained one at any temperature (Figure 32).

As the work hardening rate of aluminum is not found to be significantly dependant on temperature (Table 11) the value of percent uniform elongation is expected to decrease with increasing temperature because of an increase in the limiting cell size.

B. Dispersion Strengthened Aluminum Alloys

(a) Deformation and Recovery Processes

Brimhall et al[32] in their transmission electron microscopic studies of the deformation of internally oxidised alloys found that a high dislocation density was developed after relatively small amounts of strain. The dislocations were found to be arranged randomly rather than in cell walls if the particle distribution was sufficiently fine. A very fine cell structure was produced if the distribution of particles was somewhat coarser . These observations were interpreted as meaning that particles can act as sources as well as barriers to dislocations.

It was suggested by Brimhall et al[32] that particles may serve as barriers to dislocations in several ways. Screw dislocations may be forced to cross-slip when meeting a particle, resulting in the formation of jogs and dipoles. Edge dislocations, which cannot cross-slip, tend to bow around the particles. The screw segments which result from bowing can cross-slip, however, leaving loops and a jog in the dislocation line as described by Ashby et al[33].

The idea that particles may act as primary sources of dislocations was arrived at only on the basis of experimental observations, and no satisfactory theoretical model was proposed[32]. However, the particles may serve as secondary sources after dislocation motion is initiated, by inducing cross-slip and forming dipoles as a result.

Dispersions are also known to have a definite retarding influence on annealing processes and this is manifested in the greatly improved thermal stability of the mechanical properties of many metals which have been dispersion strengthened.

The inhibition of annealing has been generally interpreted in terms of particle restraint to the motion of boundaries[34]. One example of this type of model is that proposed by Gatti and Fullman[35] to explain the lack of macroscopic recrystallisation in internally oxidised aluminum alloys. They assumed that recrystallisation nuclei formed in a structureless matrix (i.e. portion of the matrix not containing any dislocations) as a result of thermal fluctuations. These nuclei, bounded by mobile interfaces, were depicted as growing at the expense of the surrounding strained matrix. The growth process stops if the restraining force due to surface tension of the interface or that due to particles, is equal to or greater than the driving force for boundary migration due to the stored energy difference between the recrystallised volume and the strained matrix.

When considering the retention of strength, and of an apparently cold worked microstructure to unusually high temperatures in internally oxidised copper extrusions, Preston and Grant[36] proposed that annealing was inhibited solely as a result of the interference by dispersed particles with the migration of sub-boundaries formed during deformation.

In general, annealing could be considered as occuring in two stages:-(a) the formation, from the as-deformed substructure, of a sub-grain or nucleus which is surrounded by a boundary capable of migration under thermal activation, and (b) the growth of the sub-grain by boundary migration through the remaining defect structure. Brimhall et al[37], were first to utilise transmission electron microscopy to study the annealing behaviour of dispersion strengthened alloys. They concluded that annealing inhibition by dispersions is involved in both of the above stages. They argued that in alloys containing fine dispersions, any cells formed would have a much smaller average misorientation and lower dislocation density in the cell walls as compared to pure metals. Sub-grain formation itself would thus be much less likely.

In addition to the influence of particles on the deformation mode, and therefore the type and density of dislocations in the cell walls, there can also be direct particle involvement in the dislocation rearrangement process within the walls. In cases where sub grain boundaries were observed to form in such alloys, their growth was inhibited because of the lack of a cellular distribution (or, concentration) of dislocations in the surrounding matrix. In other words the driving force for sub-grain growth is lacking when the dislocations are distributed uniformly, rather than in cells.

(b) Structure of Al-10Sb Extrusions

The Al-10Sb alloy was extruded and "annealed" at 300°C with the resulting microstructure of Figures 18 to 21. Pure aluminum, of similar mechanical and thermal history, had the much coarser microstructure revealed in Figures 13 and 14. There is sufficient evidence that annealing processes have proceeded to an advanced stage in the 300 °C extruded and annealed pure metal, which can be described as recrystallised. By contrast, in the Al-10Sb extrusion there is evidence that some of the energy of the forming process has been "stored" or retained even after prolonged heating at 300 °C. It is significant also that the AlSb particles (Figures 18 to 21) are concentrated on cell or sub-grain boundaries in the microstructure.

In the light of the work of Brimhall et al[32] it may be argued that during extrusion AlSb particles could have acted as sources of dislocations to produce a rather fine cell size at 300°C. But during subsequent annealing AlSb particles presumably acted as barriers to cell wall migration retaining the cell structure rather well.

(c) Tensile Behaviour of Al-10Sb

The 0.2% offset yield stress values for the Al-10Sb (at all test temperatures) are comparable to those of pure aluminum of similar grain size. No direct contribution of the dispersion to yield strength by an Orowan mechanism would actually be expected in this material because the AlSb particles are too widely spaced. However, it is clear that the dispersion, coarse as it may be, has resulted in a marked

increase in the resistance of deformed aluminum to recovery processes at 300°C. Thus the yield strength of Al-10Sb is appreciably greater than that of pure aluminum of identical mechanical and thermal history.

The Al-10Sb alloy was also observed to work-harden to a greater extent than pure aluminum of comparable initial grain size at all test temperatures (Figures 34 to 37) except 200°C, where neither of the two materials work hardened. This was clearly reflected in the much higher maximum true stress attained in Al-10Sb compared to the pure aluminum.

At -100°C, where dynamic recovery effects are likely to be small, the role of the AlSb dispersion is interpreted as follows. The particles of AlSb act as sources of dislocations. This, plus the inhibiting effect of the particles on the migration of dislocations to the early-formed cell walls, encourages the formation of smaller cells than are possible in the pure metal. Expressed otherwise, the limiting cell size attainable due to deformation is smaller in the presence of a dispersion. Thus the Al-10Sb alloy is able to work-harden to a higher true stress level before the driving force for sub grain formation and migration becomes great enough to end the hardening process.

The rate of work hardening of Al-10Sb decreases with increase in the test temperature (Figures 34 to 36). As the temperature is raised there is a decrease in the effectiveness of AlSb particles in preventing migration of dislocations to cell walls formed early in the deformation process. Thus the limiting minimum cell size increases with

temperature, with an effect similar to that described previously for pure aluminum. Although the initial substructure of the Al-10Sb was produced as a result of 300 °C deformation, it is apparently not appreciably coarser (or "weaker") than that produced by 200 °C tensile deformation. This is inferred from the tensile test behaviour of the alloy at 200°C, wherein necking commenced after very little plastic strain (Figure 37).

The uniform elongation results for Al-10Sb (Figure 32) are explainable in the same terms as were used previously to interpret the ductility of pure aluminum, and its dependence on grain size and temperature. Whereas pure aluminum of 2.7 or 3.5 micron grain size was able to strain very little at 20 °C before attaining the limiting cell size, and therefore beginning to neck, the Al-10Sb alloy of similar grain size was not so limited. Thus, the incorporation of a coarse AlSb dispersion has resulted in simultaneous improvements in the strength and ductility of pure aluminum.

(d) Tensile Behaviour of Overaged Al-4Cu

Extrusions of Al-4Cu, after solution-treatment and overaging, possessed a coarse grained recrystallised matrix, in which there was a very fine $CuAl_2$ dispersion (Figure 27). Any contribution which the presence of $CuAl_2$ particles might have made to the refinement of the matrix sub-structure during extrusion was subsequently destroyed by the high temperature solution treatment.

The increment in yield strength (at a low offset) for this material over pure aluminum of comparable grain size must be attributed partially to solid solution strengthening and partially to strengthening by an Orowan mechanism.

During deformation in tension, the work of Brimhall et al[32] suggests that little or no cell formation would occur at low or ordinary temperatures in the overaged Al-4Cu alloy. The very high-initial rate of work-hardening (Figures 34 to 37) in this material can be attributed to a rapid rate of dislocation generation, the particles themselves contributing by acting as sources. The concept of limiting cell size in this material probably has no meaning, so that it was possible to obtain a high true stress level without plastic instability ensuing due to cell-wall migration and the related processes discussed above. In fact relatively little necking preceded fracture of the overaged Al-4Cu extrusions, suggesting that the fracture stress of the alloy was approached throughout the specimen.

The effectiveness of the $CuAl_2$ particles in preventing any dynamic recovery processes at test temperatures as high as 100°C is also evident from the data. Only at the highest test temperature (200°C) was there an appreciable decline in strength and rate of work hardening. In fact, this might be attributable to coarsening of the $CuAl_2$ dispersion due to the combined activating effects of strain and temperature.

(e) Tensile Behaviour of Solution-treated Al-4Cu at Room Temperature

An Al-4Cu alloy quenched from a solution treatment temperature of 550 °C has been studied by Swann[27] in the electron microscope after 10% elongation. In contrast to pure aluminum, this alloy did not form any cell structure.

In the absence of a cell structure and in the presence of a supersaturation of point defects produced by quenching, the alloy can be expected to work harden rapidly, although not quite as rapidly as in the presence of a fine dispersion of a second phase.

The solution treated alloy has a higher yield strength than the overaged alloy presumably because of the much larger amount of copper in solid solution.

The maximum true stress which was attained in solution treated Al-4Cu was higher than that observed in overaged Al-4Cu. This was consistent with the lesser necking that preceded fracture in the former material.

(C) Effect of Strain Rate on Strength Properties at Room Temperature

Moon and Campbell[38] have reported that yield strength and ultimate tensile strength were not influenced or only slightly affected, by strain rate at room temperature in aluminum alloys. Trozera et al[39] have seen some increase in yield and tensile strengths when the strain rate was increased from ~~0.6 x 10^{-4}~~ ~ 1×10^{-6} sec.$^{-1}$ to ~ 1×10^{-1} sec.$^{-1}$ for pure aluminum. The strain rate dependence was very small at 20 °C or lower temperatures.

In the present investigation no distinct dependence of yield and ultimate tensile strength could be detected over the strain rate range of 0.3×10^{-4} sec.$^{-1}$ to 0.3×10^{-2} sec.$^{-1}$, at room temperature for any of the aluminum and aluminum alloys tested. This result could be expected because of the small range of strain rate involved.

V. CONCLUSIONS

1. A cell formation and growth theory due to Gay , Kelley, Weissmann and others can be used to explain satisfactorily the tensile deformation behaviour of pure aluminum as a function of initial microstructure and test temperature.

2. At low temperatures, where thermally activated recovery processes are slow, the true ultimate strength of pure aluminum is essentially grain-size independent. This is consistent with the concept of a limiting minimum size of the cells produced by deformation, this size determining the limit of work hardening, and being independent of initial microstructure in the pure metal.

3. At temperatures above about 0.25 Tm, and in the strain rate range of the present work, dynamic recovery limits the amount of work-hardening which can occur with deformation. In this case, the true ultimate strength becomes lower as the initial grain size increases. In effect, the minimum cell size attained during deformation is larger, the larger the starting grain size, because recovery (sub grain formation) occurs simultaneously with cell formation.

4. The 0.2% offset yield strength of pure aluminum appeared at all temperatures to obey a Hall-Petch relationship with initial grain size in the range 3.5 to 98 microns. However, in view of the extensive cell formation which must have ~~occured~~ occurred in the first 0.2% of strain, and because dynamic recovery probably affected the rate of work hardening at the upper end of the temperature range, it is believed that the apparent agreement with the Hall-Petch equation was largely fortuitous.

5. The observed dependence on grain size and temperature of the rate of work-hardening and uniform elongation in pure aluminum are consistent with the cell formation and migration arguments used to interpret true ultimate strengths.

6. A coarse dispersion of an intermetallic compound in aluminum has been found to retard markedly the recovery processes which result in sub-grain formation and growth. It is probable that the AlSb particles in the Al-10Sb extrusions of the present work, acted as dislocation sources, and thereby contributed to a finer cell size than was obtainable in pure alumium. In addition, the AlSb particles restricted the cell wall migration which is necessary to sub-grain formation and the nucleation of recrystallisation.

7. Al-10Sb containing a coarse dispersion of AlSb, has an appreciably higher offset yield strength than pure aluminum of similar mechanical and thermal history, for the reasons outlined in Conclusion (6). However, the yield strength was comparable to pure aluminum of similar grain size, indicating that no significant Orowan-type contribution to strength was provided by the dispersion.

8. The Al-10Sb alloy work hardened more rapidly, and showed greater uniform elongation than aluminum of comparable initial grain size. This is interpreted as reflecting the lower limiting cell size attainable in the presence of the coarse dispersed phase.

9. The high yield strength and work hardening behaviour of overaged Al-4Cu is probably best explained in terms of an Orowan-Ashby mechanism, involving the fine dispersion of $CuAl_2$ as primary barriers to dislocations.

Cell formation is not expected in such a material, and has not been observed by others. Because the strain energy of deformation is uniformly distributed in this case, instead of being concentrated in cell walls, normal annealing processes are evaded. Thus, the Al-4Cu alloy is able to work-harden almost to its fracture stress, and little necking precedes fracture.

10. The solution-treated Al-4Cu alloy is also believed to deform without any cell formation. Thus, like the overaged alloy, it work-hardens to a high true ultimate strength, and little necking precedes fracture.

11. Pronounced discontinuous yielding can occur under certain conditions in polycrystalline pure aluminum. From the present work, and that of others reported previously, it appears that the occurence of the phenomenon is dependent on annealing temperature. Only 300°C annealed aluminum has shown discontinuous yielding. It is not known what is the origin of this behaviour.

VI BIBLIOGRAPHY

1. Grant, N. J; The Strengthening of Metals (Reinhold Publishing Co.) 1964, 174.

2. Irmann, R; Metallurgia 46, 1952, 125.

3. Lyle, J. P. Jr; Metal Progress, 62, 1952, 109.

4. Nock, J. A. Jr; S. A. E. Trans., 61, 1953, 209.

5. Lyle, J. P. Jr; Materials and Methods, 43, 1956, 106.

6. Dix, E. H. Jr; Aero Engg. Rev; Jan. 1956, 106.

7. Block, E. A., and Hug. H; Sympo. Dispersion Strengthening, International Powder Metallurgy, June 1960, New York.

8. Block E. A., Met. Rev. 6, 1961, No. 22.

9. Towner, R. J; Metals Engg. Quarterly, 1, 1961, 24.

10. Collins, W. T. Jr; and Mondolfo, L. F; Tr. A.I.M.E; 233, 1965, 1671.

11. Spengler, H; Metall, 11, 1957, 384.

12. Chadwick, G. A; Progr. Mater. Sci., 12, 1963, 97.

13. Davies V de L; Jl. Inst. Metals 93, 1964-65, 10.

14. Hansen. M; "Constitution of Binary Alloys" (McGraw Hill) 1958, 130.

15. Elliott, R. P; "Constitution of Binary Alloys, First Supplement,: (McGraw Hill) 1965, 54.

16. Giesecke. G; and Pfister, H; Acta Cryst, 11,1958, 369.

17. Barker, L. J. Tr. A. S. M. 42, 1950, 347.

18. Fullman, R. L; Jl. Metals 5, 1953, 447.

19. Weissmann, S; Imura, T; and Hosokawa, N; Recovery and Recrystallisation of Metals (Interscience) 1963, 241.

20. Carreker R. P. Jr; and Hibbard W. R. Jr; Trans. A. I. M. E. 209, 1957, 1157.

21. Heidenreich, R. D; J. Appl. Phys. 20, 1949, 993.

22. Gay, P; and Kelly, A; Acta Cryst. 6, 1953, 185.

23. Gay, P; and Kelly A; Acta Cryst; 6, 1953, 172.

24. Gay, P; Hirsch, P. B; and Kelly, A; Acta Cryst 7, 1954, 41.

25. Kelly, A; Acta Cryst, 7, 1954, 554.

26. Hirsch, P. B; Horne, R. W; and Whelan, M. J; Phil Mag., 1, 1956, 677.

27. Swann, P. R; "Electron Microscopy and Strength of Crystals" (Interscience) 1963, 131.

28. Warrington, D. H; Proceedings of the European Regional Conference on Electron Microscopy, Delft, 1961, 354.

29. Stevens, R. N; Met. Rev. 11, 1966, No. 108.

30. Armstrong, R; Codd, I, Douthwaite, R.M; and Petch, N.J; Phil Mag 7, 1962, 45.

31. Warrington, D. H; J.I.S.I. 201, 1963, 610.

32. Brimhall, J. L; and Huggins R. A; Tr. A.I.M.E. 233, 1965, 1076.

33. Ashby, M. F; and Smith, G. C; Phil Mag. 5, 1960, 298.

34. Smith C. S. Trans A.I.M.E. 175, 1948, 15.

35. Gatti, A; and Fullman, R. L; Tr. A.I.M.E. 215, 1959, 762.

36. Preston, O; and Grant, N.J; Tr. A.I.M.E. 221, 1961, 164.

37. Brimhall, J. L; Klein, M. J; and Huggins, R. A; Acta Met 14, 1966, 459.

38. Moon, D. P; and Campbell, J. E; Light Metal Age 20, 1962, 18.

39. Trozera, T. A; Sherby, O. D; Dorn, J. E; Tr. A. S. M. 49, 1957, 173.